CHAPTER 5

MECHANICAL BEHAVIOUR OF THE BRINGELLY SHALE

§5.1 INTRODUCTION

At the commencement of this project, the main objective was to investigate the engineering behaviour of the natural shale rock. This has involved characterization of its index, physical, microstructural, and mechanical properties. However, as discussed previously, only limited numbers of natural core specimens were available and these were not sufficient to fully describe the behaviour of Bringelly shale. These core specimens were subjected to standard drained triaxial tests with a wide range of confining stresses and with different saturation conditions. The rationale for these tests was to investigate how Bringelly shale, which apparently has little cementation, can give *UCS* strength of up to *50 MPa* (Section 4.3.1).

In this study it was important to base the experimental program on the state of saturation of the material encountered during the sampling stage. Bringelly shale is partially saturated above the water table level which is 20-30m below the ground surface. However, below this depth, Bringelly shale is fully saturated (MacRae& Paterson, 1990). Because of the difficulties in obtaining partially saturated specimens from conventional

drilling methods and also the high cost of obtaining fully saturated shale specimens, it was decided to expand the scope of the experimental program by testing reconstituted shale specimens under saturated condition. In order to investigate the effects of structure and bonding in the Bringelly shale, it was important to acquire an understanding of the reconstituted de-structured material. To determine appropriate de-structured bahaviour, the specimens were subjected to high stresses to reproduce the low porosity.

The specimens were produced by compressing the crushed shale to specific densities under wet and dry conditions. These specimens were saturated and then subjected to a series of standard drained and undrained triaxial tests. It was expected that comparison of the natural and reconstituted specimens would provide additional information on the extent of cementation in the natural shale.

This chapter presents the equipment and procedures used to investigate the mechanical response. Results are presented within a critical state framework, and the relevance of this framework to natural shale is discussed.

§5.2 **EXPERIMENTAL PROGRAMME**

In order to obtain some base data on the strength and stiffness of the shale prior to testing the core samples, specimens from block samples were pulverized and then prepared for triaxial testing. Natural core samples were then tested and the results of both reconstituted and natural rock samples were studied. In this study, different methods were used to produce specimens for triaxial testing. Fifty five triaxial compression tests were performed on reconstituted and core samples. The tests included samples with diameters ranging from 38 *mm* to 51 *mm* and effective confining stresses varying from a minimum of *20 kPa* to a maximum of *60 MPa*. Two series of triaxial compression tests were carried out on reconstituted samples. The first series was performed on specimens prepared from slurry at confining pressures of *100, 200, 400, 700, 1000 kPa* and will be referred to as the low pressure test series. The second series of triaxial compression tests was performed at confining pressures of > *1000 kPa* and up to *60 MPa* and will be

referred to as the high pressure test series. All tests were isotropically consolidated and then sheared under drained or undrained conditions to establish the stress-strain-strength behaviour. For both series specimens were tested with a range of over-consolidation ratios. Due to the wide range of the hydrostatic pressure used for conducting these tests, it was necessary to employ different sets of triaxial testing equipment to suit the pressure and the subsequent deviator load during the test. Figure 5.1 shows a flow chart giving details of the test program.

§5.2.1 **Specimen preparation method**

Three forms of shale specimens were produced from blocks and core samples. The specimens were made of two types, the first is reconstituted shale, and the second is natural shale. The first type includes two forms, slurry and dry press forms, while the second type includes the natural shale. Details of the procedures to prepare the different specimen types are given below.

§5.2.1.1 **Natural shale**

A. **Core form**

Cylindrical specimens were obtained from boreholes located at Kemps Creek and Badgerys Creek sites (Chapter 3). Core runs were drilled by using conventional drilling with water flush. The drilling of the core runs was carried out in a direction perpendicular to the bedding plane. The main lithology dominating the specimens was claystone and siltstone. The rock quality designation *RQD* of the two runs from *KC* and *BC* sites were calculated according to the following formula:

$$RQD = \frac{\sum L_S}{L_T} \times 100 \qquad (5.1)$$

in which

L_S = Sum of lengths of core sticks > 10 *cm* long

L_T = Total length of core run

Based on the rock mass classification proposed by Deere et al. (1988), the rock quality of Bringelly shale measures 9-11% and would be classified as very poor.

Flow chart of experimental program

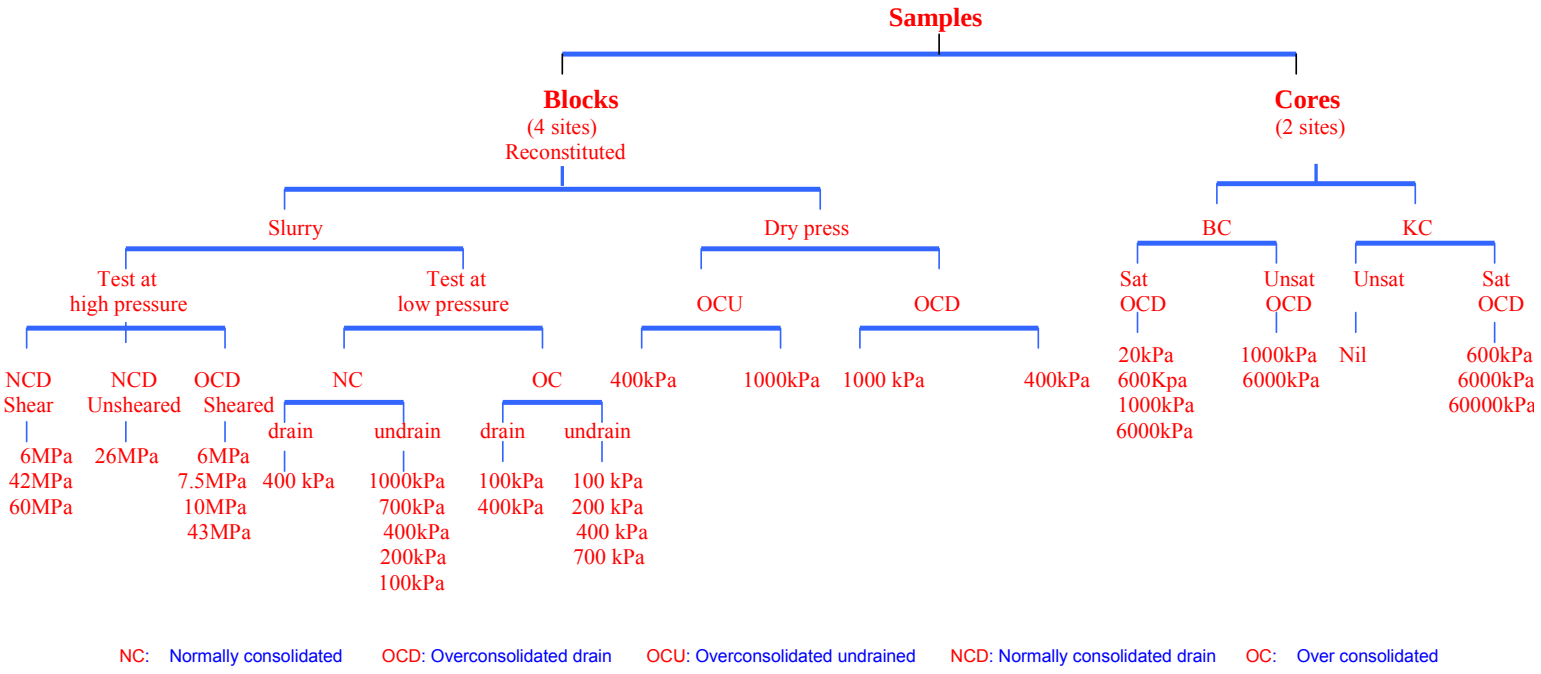

Figure 5.1 Flow chart showing triaxial testing program for Bringelly shale

Due to the poor quality, only few cores with a maximum length of *130 mm* from Kemps Creek (*KC*) and cores with a maximum length of *110 mm* from Badgerys Creek (*BC*) could be selected for triaxial tests. These specimens were kept at their sampled moisture content by coating them with a moisture sealant called Valvoline Tectyle and then by wrapping them in a thin plastic film. The treated specimens were then placed in a box and kept in the laboratory at steady temperature until further processing.

Prior to testing, specimens were trimmed to the required lengths using a rough sandpaper. A diamond saw could not be used for this purpose as the material chipped off and disintegrated after a few cuts / passes. Fine sandpaper was used for grinding both ends of each specimen so that squared specimens could be produced. The diameters of specimens from *KC* and *BC* were approximately *50 mm* and *45 mm* respectively. The diameter and height of the specimens were measured with a vernier caliper according to the ISRM suggested methods. The diameter of each specimen was measured to the nearest 0.1 *mm* by averaging two diameters measured at 90 degrees to each other at about the mid height and the upper and lower ends of the specimen. The average diameter was used for the cross-sectional area calculation. The height of each specimen was measured to the nearest *0.1 mm* by averaging two diametrically opposed height measurements.

§5.2.1.2 **Reconstituted shale**

A. **Slurry form**

These specimens were produced by pulverizing fresh shale and reducing it to a powder. Material passing a *0.425 mm* sieve was used in preparing the samples. The slurry sample was prepared in a plastic container by thoroughly mixing a pre-determined amount of the crushed material with a pre-determined volume of distilled water to give a moisture content greater than the liquid limit. In order to produce a uniform reconstituted sample, a device, shown in Figure 5.2, was built in the soil mechanics workshop to help the process of filling the mould with slurry and produce air free specimens in reasonable time. This was achieved by controlling the position of a piston in the mould so that slurry could be placed without trapping air. The slurry

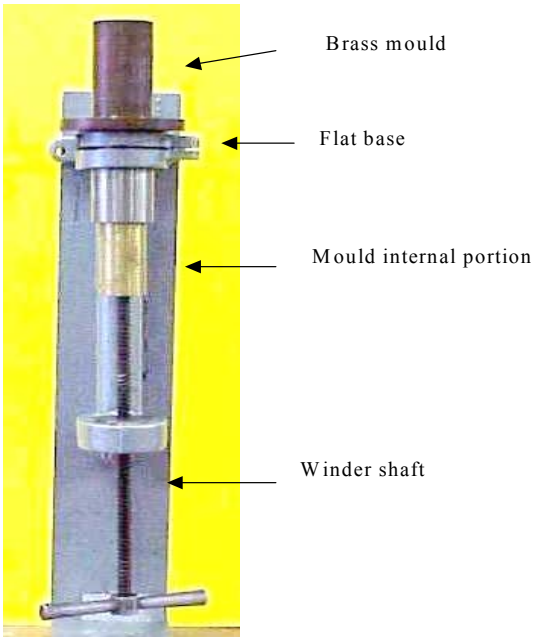

Figure 5.2 Mould with piston used to reduce air entrainment

of pulverized shale and distilled water was placed layer by layer into a 38 *mm* diameter by 80 *mm* height brass mould placed on the filling device. To facilitate moulding, the slurries were made with water contents of about *62%*. This value is about *1.8* times the liquid limit of the natural material. Before moulding, some petroleum jelly was applied to the mould's internal wall to reduce shear stresses at the contact with the mould during consolidation and also to ease subsequent extrusion. Prior to filling, a porous stone with a

filter paper on the top was placed at one end of the mould. At the end of filling, the mould was closed from the top end by a filter paper and a porous stone. The soil was then compressed one-dimensionally by dead loads applied to a hanger to give a vertical stress σ_v of $80\ kPa$ (Figure 5.3). In order to maintain a good degree of saturation, samples were kept under water. Samples were usually removed after *72* hours to be mounted in the triaxial machine.

B**. Dry pressed form**

The purpose of using a dry pressed method (at field water content) was to rapidly produce samples with low porosities. A pre-determined mass of pulverized shale

Figure 5.3 Consolidation of the reconstituted specimen under dead weight

powder was placed between the top and bottom rams of a split-cylindrical steel mould (Fig. 5.4). In order to eliminate adhesion between the powder and the surface of the 38

mm diameter mould, the surface was smeared with grease. Axial load was then applied by a rigid loading frame with a $300\,kN$ capacity servo-controlled hydraulic actuator. The load was increased until the specimens were compressed to reach a target void ratio of *0.15*.

For this target void ratio, the axial stress required was approximately 30 *MPa.* The axial load was then removed and the mould split open to extract the soil sample. Following the removal of the sample, it was immediately wrapped in plastic wrap and then placed in a plastic bag and sealed. All samples were stored at room temperature until further testing.

The mass of crushed shale required was calculated knowing the final height of the sample, which was chosen to suit the required standard height to diameter ratio for triaxial testing. This meant that no cutting or trimming was needed prior to a test.

Figure 5.4 Split mould used in reconstituting specimens at low porosity.

§5.3 EQUIPMENT DESCRIPTION AND DATA AQUISITION

More than 55 triaxial compression tests have been carried out with confining stresses varying from *20 kPa* to *60 MPa*. This made it necessary to employ two different sets of triaxial equipment, the first set was used to perform tests at low confining pressure up to 1.5 *MPa*, while the second set was arranged for performing tests at higher confining pressures up to 60 *MPa*. For both pressure ranges the equipment was essentially the same and consisted of a triaxial cell, pore pressure transducer, axial displacement transducer, a personal computer, two digital controllers that provide cell pressure and back pressure, and a rigid loading frame for applying axial load. For the high pressure tests, a rock cell with 70 *MPa* was used together with a *GDS* pressure-volume controller with 64 *MPa* capacity for the confining pressure. The rock cell was also used to measure unconfined compressive strength and axial strain of natural rock core. Pictures to illustrate the general view of the triaxial arrangement and details of different systems used for these tests are described in the following sections.

§5.3.1 **Low pressure triaxial testing system**

A triaxial apparatus with a cell pressure capacity of 1.7 *MPa* was employed in this system. Cell and back pressures were provided separately by two 2 *MPa GDS* digital controllers. Axial load was provided by a Tritech compression machine with a capacity of 50 *kN* (Figure 5.5). The majority of the tests on reconstituted shale with effective stresses ranging between 20 *kPa* and 1000 *kPa* were carried out using this system.

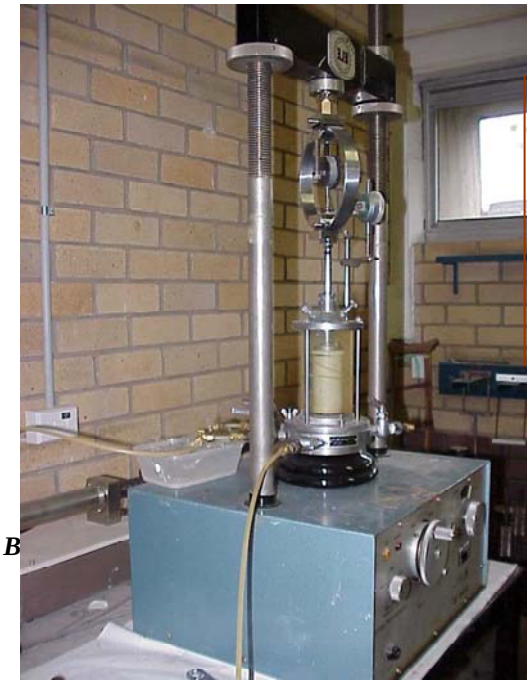

Figure 5.5 A conventional low pressure triaxial test cell

§5.3.2 **High pressure triaxial testing system**

All tests of reconstituted specimens at confining stresses greater than 2 *MPa* were performed using a high pressure triaxial cell. Several load frames were used depending on the confining stress and specimens, but most tests were conducted in a frame with a capacity of 250 *kN*. The high pressure tests were performed in a stiff Model *10* triaxial cell with 1-way drainage and a cell pressure capacity of 70 *MPa*. A *GDS* digital controller with a capacity of 64 *MPa* was used to provide the cell pressure with effective confining stresses up to 60 *MPa*. The high pressure test arrangement equipment is shown in Figure 5.6.

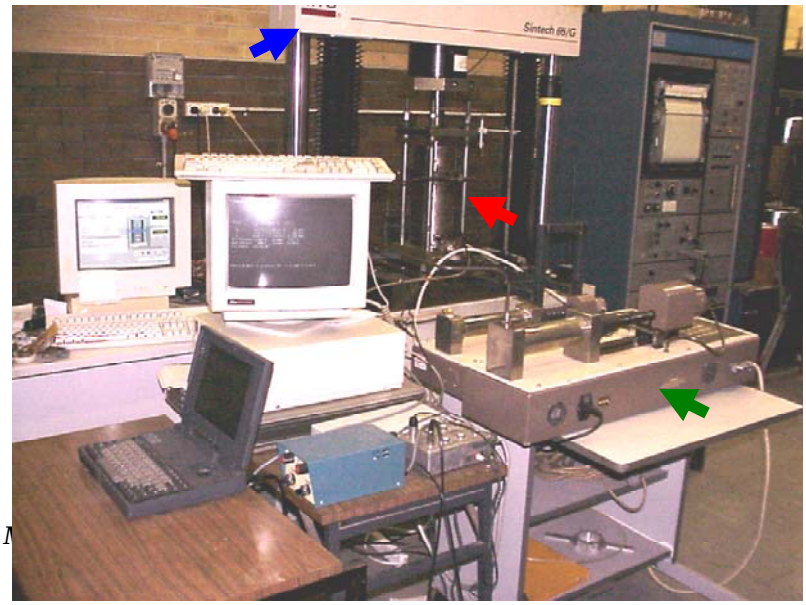

Load frame Triaxial cell GDS

Figure 5.6 Overview of equipment used for high pressure triaxial tests

§5.3.3 **Measuring devices and data control**

Based on the applied pressure for each test, different measuring load devices were used. For tests performed in the Tritech loading frame, axial loads were measured by proving rings which were instrumented to provide an electrical output for automated data logging. For tests with pressures less than 1000 *kPa*, a proving ring with a capacity of 10 *kN* and a resolution of approximately 3.5 *N* was used . For tests with confining pressures between 1000 and 8000 *kPa*, an external load cell connected beneath the cross-head with a capacity of *50 kN* and a resolution of approximately 10*N* was used. For the higher pressure tests, the axial load was provided by an Instron Servo-Controlled testing machine (*Sintech*) with a capacity of 250 *kN*. The axial load was measured by a model 661.23D-01 load cell installed beneath the actuator with a resolution of 15 *N* .

Depending on the magnitude of the pore pressure generated, two types of pore pressure transducer were used; a Druck PDCR 960 2 *MPa* transducer, and a Bell& Howell BHL/4400 10 *MPa* . The pore transducer was connected to the cell base outlet close to the specimen. Each had a resolution of approximately 0.5 *kPa*. In drained tests, a *GDS* back pressure controller was used to measure volumetric changes. Cell, pore pressures, and volume changes during triaxial tests were controlled and measured by *GDS* controllers that were operated under computer control. Their detailed descriptions have been discussed by Menzies (1988).

Axial displacement was measured by a Hewlett Packard DC-DC *LVDT* mounted externally to the proving ring and bearing on the top of the cell. It had a range of ±33 *mm* and a resolution of approximately 0.006 *mm*.

For all triaxial high pressure tests, the axial load was transmitted through the upper loading platen to the specimen. The upper platen was spherically seated to the ram in an attempt to eliminate end-moments being applied to the specimen, particularly in cases where the flat ends of the cylindrical specimens were not exactly parallel. For reconstituted specimens at low pressure, the axial load was transmitted through the lower loading platen to the specimens.

All test arrangements had automated data logging programs to record the progress of the tests. Software written in Quick Basic was used to record and control the tests carried out in high and low pressure modes. Modifications to the software were made to allow for the logging of external devices or other components and also for changing the time interval of reading data, so that copying unnecessary data could be avoided.

The same data acquisition system has been used for the low and high pressure tests. This has included an amplifier/signal conditioner, a 16 bit A-D converter and an IBM compatible computer. The raw data recorded include readings of axial load, axial displacement, pore pressure, cell pressure, back pressure, and time. After a test, these readings were than processed using the appropriate formulae to determine deviator stress, mean effective stress, axial strain, and volumetric strain. Other parameters such as the water contents before and after a test and specific gravity were also recorded and used in calculations.

The frequency at which data were stored was based on the increments of deviator stress, axial strain, volumetric strain, and time. This varied from test to test depending on stress level and sample preparation type.

§5.3.4 **Calibration of equipment**

All devices were calibrated to determine the accuracy and reliability of the data. Additional checks were performed to ensure there were no leaks in the drainage system or through the membrane.

The *GDS* controllers were calibrated against a dead weight standard, and then were used to calibrate the pore and cell pressure transducers. The *GDS* was used to control pressure, but outputs from independent transducers were used for test analysis, except for the high pressure tests where the cell pressure was taken from the *GDS*.

The proving ring was calibrated for the range from zero to 5.5 *kN*, as this upper value was sufficient to fail the sample tested at low pressure (≤ 1000 *kPa*). Figure 5.7 shows a typical variation of load with output voltage. It is clear that the relationship is linear and the equation of this line was used in the computer program for voltage conversion to load.

For the purpose of calibration of the displacement transducer (*LVDT)*, a calibration fixture was used (Fig. 5.8a). The fixture used a micrometer measuring the displacement vertically. The micrometer could produce direct displacement of the core. The output signals were in the range of ±5V full-scale output. The output of the displacement transducer is plotted in Figure 5.8b. The slope of the trend line in the graph was used in the program to convert voltage readings to displacement measurement during the tests.

In the low pressure tests, the pore pressure transducer (*PPT*) that was mounted on the cell base had a working range of zero to 2 *MPa*. The output voltage was amplified to

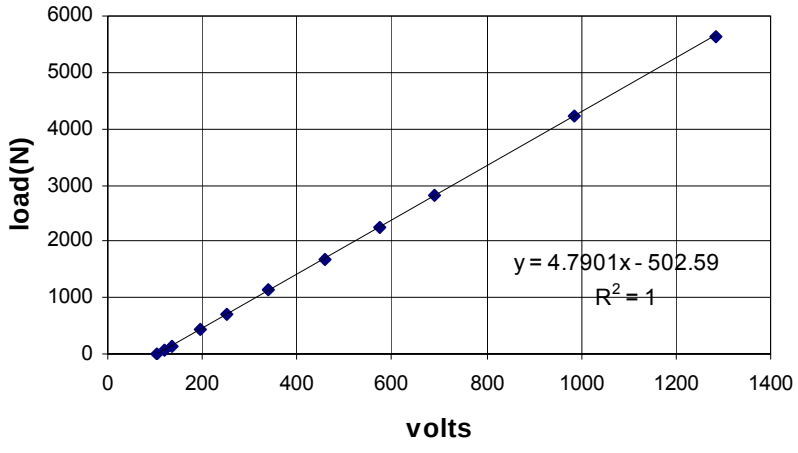

Figure 5.7 variation of load with output voltage for proving ring displacement transducer

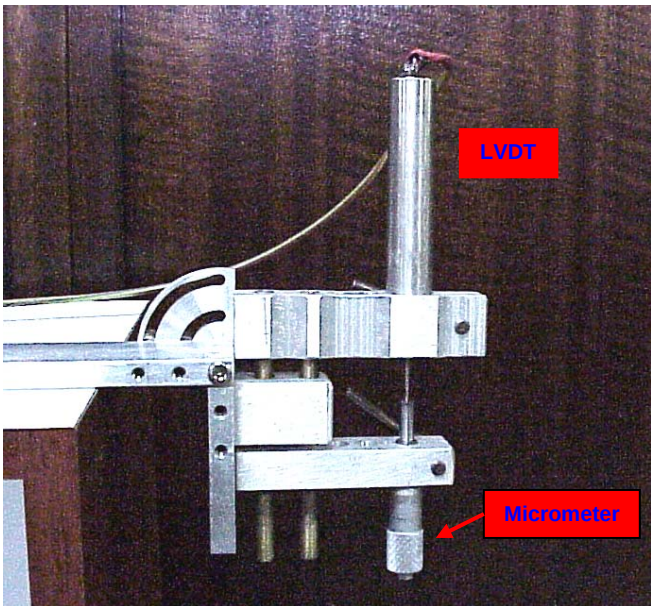

(a)

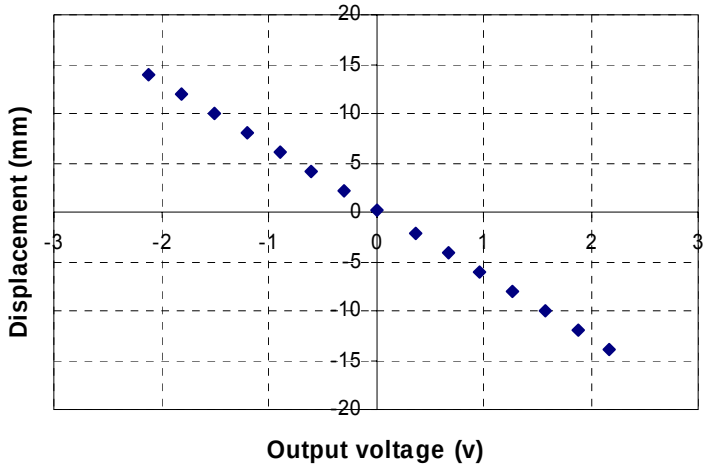

(b)

Figure 5.8 Calibration set up for LVDT (a) and results for displacement transducer

give -3V to +5V output for a pressure change from zero to 2 *MPa*. For calibration of the *PPT* the cell was filled with water, then the pressure of the cell was gradually increased by a *GDS* cell pressure controller in steps of 50 *kPa* whereas the maximum pore pressure was adjusted to 300 *kPa*. Both pore pressure and output voltages were recorded simultaneously.

The results are shown in Figure 5.9. The calibration confirms a linear relationship between pore pressure and output voltage.

Prior to tests, it was necessary to ensure that both cell and back pressure *GDS* will have the same readings when measuring the same pressure. A relationship between the reading responses of the two devices was plotted on Figure 5.10. The figure shows a linear relationship with a gradient ~ 1 and an error of about 2 *kPa* in every 1000 *kPa*. In the high pressure tests the cell pressure *GDS* could not resolve to better than ±16 *kPa*. In order to avoid suctions a minimum 32 *kPa* difference was required between cell and back pressures during sample preparation.

As part of the routine data processing, the standard correction for cross-sectional area which assumes the specimens remain cylindrical was applied for all tested specimens.

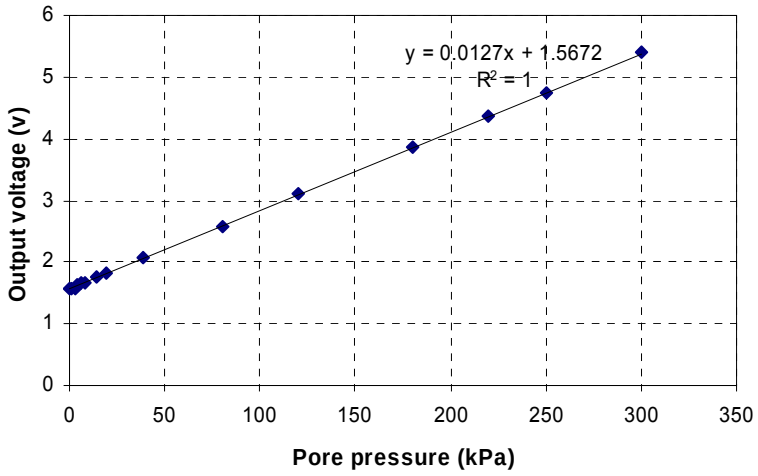

Figure 5.9 Calibration results of Pore Pressure Transducer

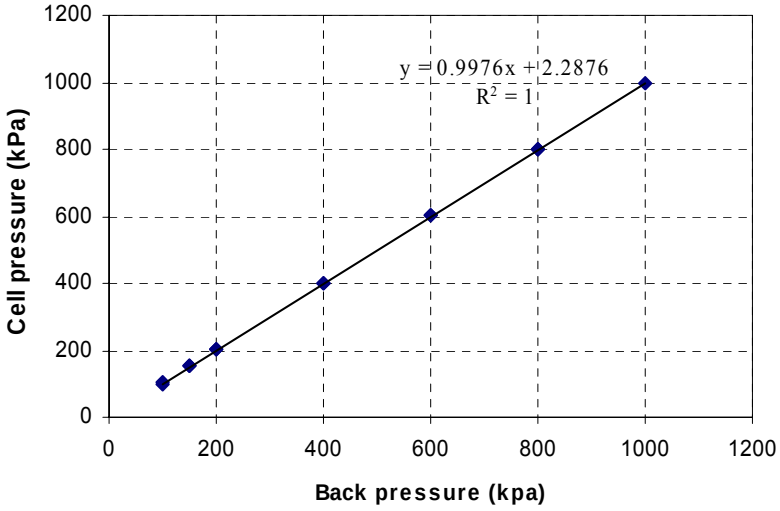

Figure 5.10 Measuring the readings at the same applied pressure

§5.4 **TRIAXIAL COMPRESSION RESPONSES**

The equipment used for these tests has been described in Section 5.3. The effects of effective confining stress, structure, and saturation on the drained and undrained triaxial compression responses of the three different types of specimens are presented in this section.

The section will also explore the assumption of many simple critical state soil mechanics models that sections through q, p', e space at constant e are similar. These sections can be studied by plotting q and p' normalised by the equivalent p'_e on the *INCL* at the same e. The following discussion has followed the terminology used in critical state soil mechanics (e.g. Atkinson and Bransby, 1978), using the Roscoe surface and Hvorslev surface to describe parts of the state boundary surface.

§5.4.1 **Experimental method**

Reconstituted specimens with a height to a diameter ratio of about two were extruded manually from the brass mould. Height and diameter of the specimen were measured to the nearest 0.01 *mm* prior to assembling of the triaxial cell. Before mounting the specimen, all the drainage lines and the pore pressure transducers were filled with distilled de-aired water. Porous discs were first placed into an ultrasonic cleaner to remove any fine particles. The discs were then saturated under vacuum (28 *mmHg*) for 15 minutes. In every test filter papers were placed between the base of the specimen and the porous disc and also between the top of the specimen and the porous stone followed by the top cap. The specimen was then covered with a membrane made of latex rubber.

For the low pressure tests with confining stresses less than *1000 kPa*, each specimen was covered by a single 0.25 *mm* thick membrane. For the high pressure tests, reconstituted specimens were protected from cell water by using a *0.8 mm* thick membrane. For the

natural core specimens, *1.2 mm* thick membranes were used to minimize possible damage and subsequent leakage due to the sharp edges at the top and base of the specimen. It was found from experience that 1.2 *mm* membranes were required for all tests on the natural core specimens. When thinner membranes were used, leaks developed due to membrane penetration effects particularly at the commencement of failure where pressure, acting on sharp edges resulting from the shear plane, has punctured the membranes (Fig. 5.11). This often led to complete loss of the specimens. To avoid such incidents, two rubber bands 12 *mm* thick and 15 *mm* wide were cut and placed around the circumferential contact of the top and the bottom specimens with the top cap and the pedestal respectively. Membranes were then sealed to the base and the top cap with four "O" rings, two at the top and two at the bottom to prevent any possible leakage. At the end of setting up the specimen, the cell cover was closed and then filled with distilled de-aired water.

§5.4.1.1 **Saturation stage**

After the cell was filled with water, the loading ram was lubricated with silicon oil and was adjusted so that proper seating and alignment of ram with the top cap could

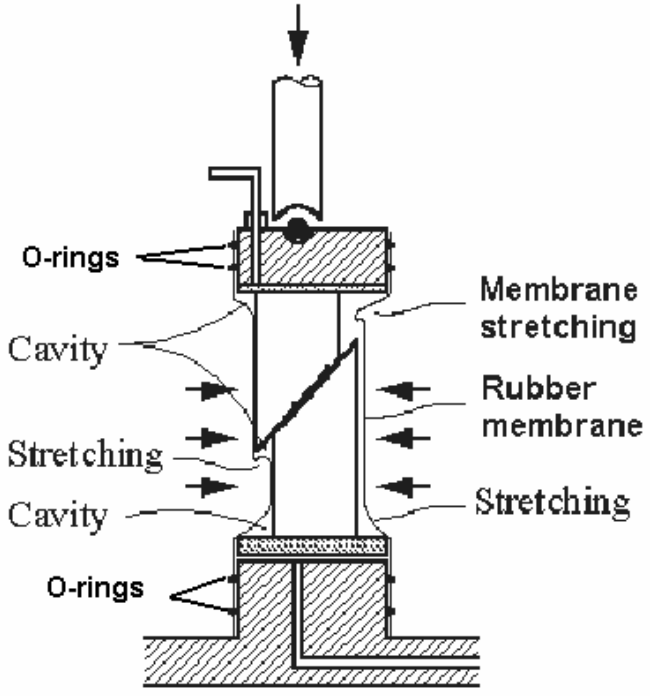

Figure 5.11 Influence of geometry on the rubber membrane during shearing (modified from Lade & Hernandez, 1977)

be ensured. Then a confining stress of 30 *kPa* was applied. Saturation of reconstituted slurry specimens was carried out by applying a back pressure of 500 *kPa* which was found to be sufficient to drive all the air into solution (Bishop and Henkel, 1962). The back pressure was increased by ramping both cell and back pressure while keeping the effective confining stress constant at 30 *kPa*. Specimens were left for up to one week to saturate.

In order to achieve a maximum degree of saturation particularly for specimens with low porosity (dry pressed and natural core specimens), compressed carbon dioxide gas was flushed through the drainage lines and specimens prior to applying the back pressure. Although the main objective of using this technique was to speed up saturation because of the greater solubility of CO_2 in water (e.g. Bishop and Henkel, 1962), the CO_2 was found to have little effect on the *B*-values achieved for dry-pressed specimens.

To prevent the swelling and subsequent disintegration of natural specimens higher confining stresses were used during saturation. Tests carried out by Itakura (1999) on specimens from *KC*, showed partial disintegration during saturation at an effective stress of *200 kPa*. In the current studies, after a few trial tests on the material, it was found that increasing the effective stress to *600 kPa* was sufficient to reduce the swelling as discussed in Section 4.4.2 and hence to maintain the integrity of the specimen during saturation.

Saturation was checked by calculating the *B-value* (Skempton,1960) while drainage was not allowed. It was calculated from the following relationship:

$$B = \frac{\Delta u}{\Delta \sigma_3} \qquad (5.2)$$

where

Δu : the change in the pore pressure due to a change in the cell pressure

$\Delta \sigma_3$: the change in the cell pressure

The *B* value for specimens produced from a slurry was between 94-96% while the *B* -value never exceeded 62% for those specimens obtained from the dry press and conventional drilling. These values, are believed to be indicative of the high stiffness of the shale specimens, and not that the specimens were incompletely saturated. *B*-values were also used to assess and estimate stiffness, assuming that specimens were saturated. This also suggests that the specimens were saturated despite the low *B*-values measured. Full saturation ensures that the volume change measurements reflect the true void volume change of a specimen in drained tests, and avoid the complexity of "undrained" testing on unsaturated specimens. If samples are saturated the void ratio *e*, may be simply determined from the measured moisture content, *w*, since the two quantities are related by the specific gravity of a specimen G_s.

§5.4.1.2 **Consolidation stage**

Following saturation, a series of incremental changes to the cell pressure were applied to the specimens, and in some tests two cycles of loading and unloading were carried out. In the consolidation stage the specimen is consolidated isotropically under a confining pressure by allowing water to drain out into the back pressure *GDS*. As a result, the pore water pressure gradually falls until it virtually equal the back pressure. This can be observed from the readings given by the pore pressure transducer and the *GDS* back pressure. In this study, the staged consolidation technique was used to raise the stress to the required confining stress. Each consolidation stage was considered to have been

completed when the volume change - time plot, showing on the computer screen, indicated that the specimen had reached a stable state, with only very small volume changes occurring over time. Multi-stage consolidation was used for all forms of specimens to ensure full primary consolidation in the shortest possible time.

Consolidation tests are often carried out on clays, but only rarely on soft rocks and cemented soils because of their low porosities (Huang, 1994). Consolidation refers to the time dependent dissipation of pore water pressure and associated deformations. Consolidation tests are often performed to investigate the stress-strain-time relationships of soils and also to be able to study the influence of consolidation history on the mechanical behaviour of the soil during shearing. In this study, the term consolidation is used to refer to the consolidation of the reconstituted specimens while the term reloading is used to refer to the consolidation of the natural core specimens. For all tests, normal consolidation and overconsolidation were applied according to the experimental program (Section 5.2).

For the low pressure test series, it was observed that consolidation occurred relatively slowly. The volume change – time plot indicates that primary consolidation took an average of 26 hours for stresses that were close to the apparent preconsolidation stress, and approximately 18 hours for stresses greater than 200 *kPa*. A typical isotropic consolidation response of a specimen from the low pressure series is shown in Figure 5.12.

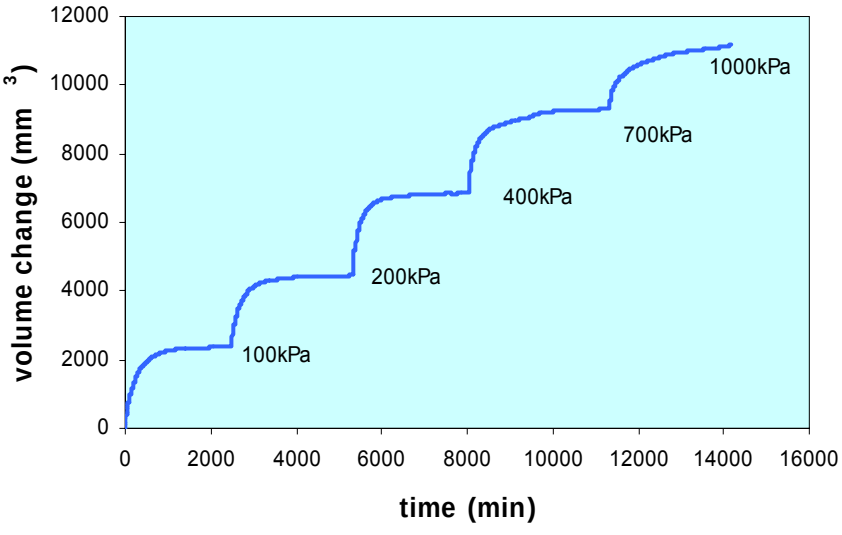

Figure 5.12 Typical staged consolidation curve for low pressure test series

For the core specimens, the time for reloading and dissipation of the pore pressure was shorter compared to that taken for the reconstituted specimens. This difference in time is due to their high stiffness, and low porosity. It has been suggested above that the core and dry pressed shales were saturated, however, if this was not the case consolidation would be expected to occur more rapidly.

Parameters such as time to failure (t_f), coefficient of permeability (k), the coefficient of volume change (m_v), and coefficient of consolidation (c_v) were determined from the graphical results of the isotropic consolidation tests, following procedures outlined by Head (1986).

Based on the data obtained from the consolidation curves, the coefficient of consolidation (c_v) was determined from the value of t_{90} that is the time to reach 90% consolidation. The following equation was used:

$$c_v = \frac{0.848 \times h^2}{t_{90}} \qquad (5.3)$$

where h is the length of the maximum drainage path, which in the case of drainage from both ends is the height of the specimen (H) divided by two. Two way drainage was used in most low pressure test series, while one way drainage was used for all high pressure tests where $h = H$.

The c_v values determined from 5.3 were then used to calculate the coefficient of permeability k using the following expression (Head, 1986):

$$c_v = \frac{k}{3\gamma_w} \times \frac{\Delta p'}{\Delta \varepsilon_v} \qquad (5.4)$$

For clarity, a summary of average data from normally consolidated reconstituted material at different stress levels is shown in Table 5.1.

The data show that c_v values range from 0.02 to 0.065 mm^2/sec and vary with the pressure applied. The coefficient of consolidation varies by a factor of 3 over a wide range of stresses for reconstituted specimen forms. An increase in c_v is often associated with an increase in the consolidation stress. A consistent pattern of

Table 5.1 Calculated parameters from isotropic consolidation data on reconstituted slurry specimens

Stress level (*kPa*)	**c_v(*mm^2/sec*)**	**m_v (*m^2/N*)**	**k (*m/sec*)**	**$\Delta p'/\Delta \varepsilon_v$ (*kPa*)**
1000	0.020	3.3×10^{-6}	2×10^{-9}	0.3×10^{3}
6000	0.043	2.6×10^{-7}	3.4×10^{-10}	0.38×10^{4}
60,000	0.065	1.5×10^{-8}	3×10^{-11}	0.65×10^{5}

decreasing permeability associated with increase in the applied stress level was also observed. Attempts were made to estimate the maximum excess pore pressure particularly for *OC* tests performed with 1 way-drainage. The 1-dimensional equation for consolidation was solved numerically using finite difference equations to determine the loading rate that allows the generation of a minimum excess pore pressure. The time determined for the tests using one way drainage was reduced to 25% when 2-way drainage tests were performed.

§5.4.1.3 **Shearing stage**

Immediately after the end of isotropic consolidation, the loading ram was brought into contact with the top cap. The specimens were then axially loaded to failure in either drained or undrained conditions. The maximum rate of loading was calculated using the method presented by Head (1986) based on the type of drainage and testing conditions.

The time for failure t_f was calculated from:

$$t_f = 0.51 \times t_{100} \quad \textit{for undrained, and} \qquad (5.5)$$

$$t_f = 8.5 \times t_{100} \quad \textit{for drained} \qquad (5.6)$$

For example, in the low pressure test series where two way drainage was used, the loading rate was 0.1 *mm/min* for undrained conditions and 0.003 *mm/min* for drained conditions. These rates were slower than what Head recommends to allow for stabilizing the pore pressure within the sample during undrained tests and the dissipation of excess pore water during drained tests. Following the same approach, the loading rate for the drained high pressure test series with only 1-way drainage, was chosen to be 0.0012 *mm/min*.

For the dry pressed samples rates of 0.006 and 0.03 *mm/min* were used for drained and undrained tests, respectively. It was important to commence the shearing stage immediately after the loading ram had come into contact with the top platen. This was to consistently allow for the effects of creep that otherwise would have occurred between the end of consolidation stage and the period before the ram came into full contact with the sample.

During shearing, each specimen was loaded to failure at a constant rate of axial deformation. Failure was defined as the point at which the peak deviator stress occurs. Whenever possible, shearing was continued beyond the failure condition, until an ultimate or residual shear state was reached. Cell and pore pressure, axial load and deformation, and volume change, were all monitored throughout each test.

At the completion of shearing, each specimen was unloaded at the same loading rate, and for the high pressure tests cell pressure was reduced to *30 kPa* effective confining stress in an effort to equalize the excess pore pressure, so that the water content, which for some specimens was very low, would not be unduly influenced by sucking water out of the porous discs. The specimens were then removed and quickly weighed before being placed in an oven to dry at $105^{o}C$. The moisture content was then determined.

§5.4.2 **Data corrections**

The final dry and wet masses of the specimens after the end of shearing were used to calculate parameters such as initial volume of the specimen V_o, volume of solids V_s, volume of water V_w, weight of solid w_s, and weight of water w_w. The specific volume v, and changes in the volume of the specimens at each stage of consolidation were calculated from the volume change measured by the *GDS* controller. Specific volume was calculated by dividing the total volume of the specimen by the volume of the solids as follow:

$$v = \frac{V_w + V_s}{V_s} \qquad (5.7)$$

The reduction in the specimens' heights due to isotropic compression was determined from the volume change measured by the *GDS* controller. The height of the specimen after consolidation H_c was calculated assuming the deformations were isotropic, as follows:

$$H_c = H_o - \frac{V_{GDS} \times H_o}{3V_o} \qquad (5.8)$$

where

V_{GDS} is the volume change, *and*

H_o and V_o are the initial height and volume, respectively

The diameter of the specimen after consolidation D_c can be determined similarly.

The axial and volumetric strain during shearing were calculated as follows:

$$\varepsilon_a = \frac{\Delta H}{H_c} \qquad (5.9)$$

$$\varepsilon_v = \frac{\Delta V}{V_c} \qquad (5.10)$$

where

ΔH and ΔV are respectively, the change in height and volume during shearing, *and* V_c is the volume at the end of consolidation

Deviator stress q', was determined using:

$$q' = \frac{F}{A} - u \qquad (5.11)$$

where F is the axial load and A is the corrected cross-sectional area, and u is the pore pressure. This area was calculated using the following equation:

$$A = A_c\left(\frac{1-\varepsilon_v}{1-\varepsilon_a}\right) \qquad (5.12)$$

where A_c is the cross-sectional area of the specimen at end of consolidation. Based on this corrected area, mean effective stress p' can also be calculated as follow:

$$p' = \frac{\sigma_1' + 2\sigma_3'}{3} \qquad (5.13)$$

where σ_1' and σ_3' are the major and minor effective stresses respectively.

In some high pressure tests, specimens with 45 *mm* diameter were tested in a triaxial steel cell with 51 *mm* ram diameter. It was important then to make a correction to eliminate any additional stresses. The following equation was used:

$$q' = \frac{F}{A} - \frac{A_{ram} \times \sigma_3}{A} - u \qquad (5.14)$$

where

A_{ram} is the ram cross sectional area, *and*

σ_3 is the total confining stress

§5.4.3 **Reconstituted results**

§5.4.3.1 **Isotropic compression**

One of the aims of the experimental investigation in this study was to describe the shale behaviour with reference to the critical state framework (Schofield and Worth, 1968). One of the assumptions of most critical state models for clay soils is that isotropic compression may be described by an equation of the form:

$$v = \mathrm{N} - \lambda \ln p' \qquad (5.15)$$

where

v is the specific volume, λ is the slope of the compression line, and
N is the specific volume at mean effective stress $p' = 1\ kPa$

Similarly, the unloaded response can be written as:

$$v = v_\kappa - \kappa \ln p' \qquad (5.16)$$

where

v_κ is a constant and κ is the slope.

Typical responses are shown in v : lnp' in Figure 5.13 for reconstituted slurry and dry pressed specimens. Representative data are shown in Figure 5.14a in e : lnp' and in Figure 5.14b in $ln\ e$: $ln\ p'$. Although it has been suggested (Butterfield, 1979) that improved linearity in the isotropic response occurs when plotting logarithms of both v and p', this was not observed for the reconstituted shale, which gave non-linear responses in all the various representations. However, it was found that Eq. 5.15 gave a good representation of the data for stresses from 100 *kPa* to 30,000 *kPa*. The slope of the *INCL*

for p' < 100 *kPa* was not investigated in this study. It was found that the *INCL* is described well for the range 10 *MPa* ≤ p' ≤ 60 *MPa* by a hyperbolic function given by:

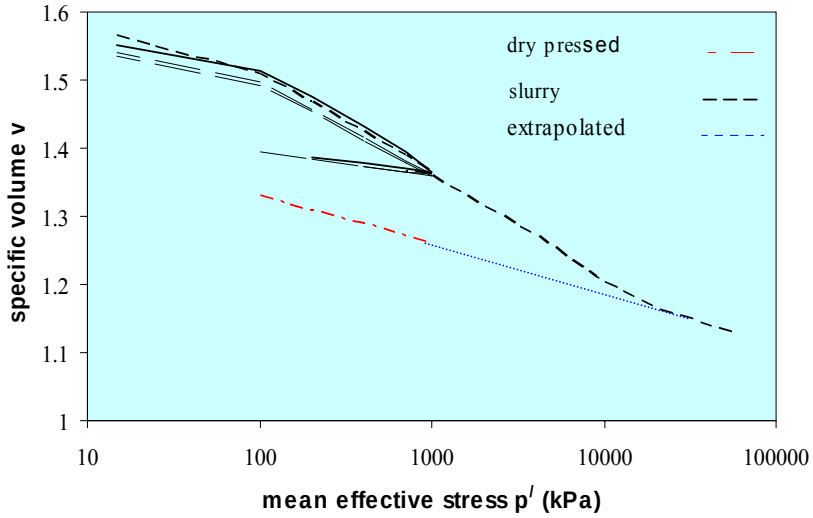

Figure 5.13 Isotropic compression responses

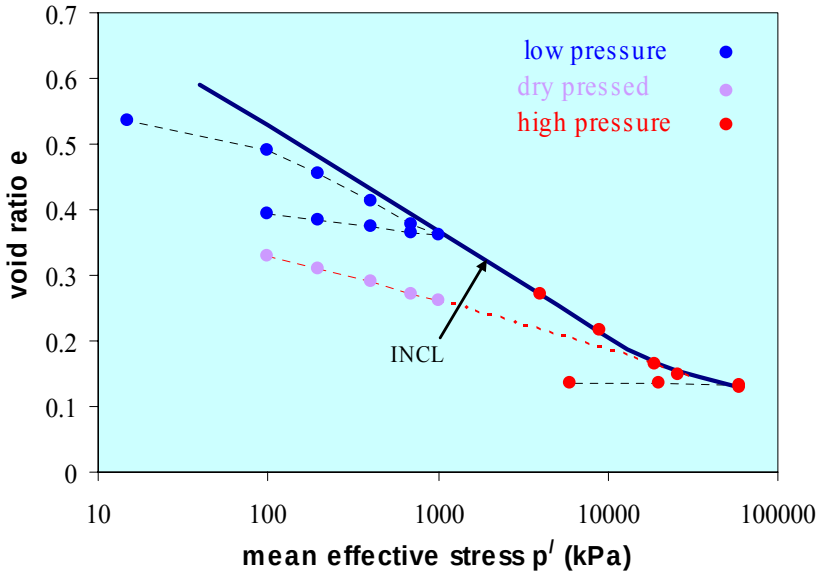

(a)

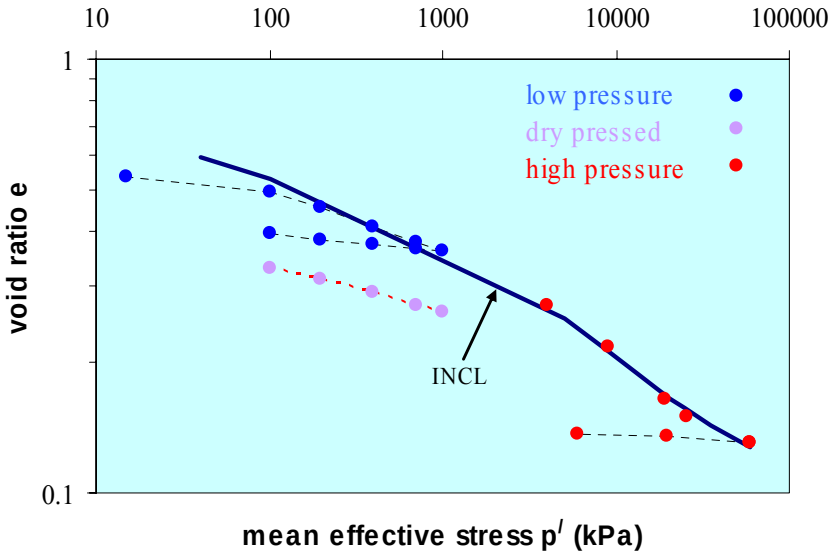

(b)

Figure 5.14 Isotropic compression of reconstituted Bringelly shale in: (a) semi-log scale, and (b) log-log scale

$$e = \frac{A}{(\ln p' - B)} \qquad (5.17)$$

where A and B are constants that can be chosen so that *INCL* is continuous with no change of slope at p'=*10,000 kPa*. No data on the *INCL* were available for pressures > 60 *MPa*.

It may be noted that responses of slurry specimens are repeatable with only a small range of v for a given p' shown in Figure 5.13. The parameters λ, N, and κ are constant within the range 100–10,000 *kPa* and are given by 0.07, 1.85, and 0.009 respectively. A and B

are constants and equal to 1.4 and 1.2 respectively. It may also be noted that the value of κ reduces from 0.009 at 1000 *kPa* to 0.0013 at 60 *MPa*.

The isotropic response is linear over a wide range of stress, as reported for many other clays and clay shale (Skempton, 1970; Morgenstern, 1977; and Yang et al. 2004). Data on the compression response at high stress is very limited. For example, Skempton's data is based on interpretation of void ratio with depth from in-situ deposits. Yang (2004) described the responses between void ratio and vertical effective stress of clay shale from the North Sea in the context of a relationship between clay content and compression coefficients where void ratio was significantly reduced when subjected to 40 *MPa* vertical effective stress. It is thus unclear whether the curvature in the *e* : *ln p*' response is a consequence of the high stress level or the unusually low void ratios achieved for this material. It is believed that the low void ratio has required substantial particle alignment and this limits further compression, and hence that the low void ratio has a significant effect on the flattening of the compression response.

The samples prepared by the dry pressed method had experienced a maximum effective stress of approximately 30 *MPa* and a minimum void ratio of 0.15 during preparation. However, after unloading and extrusion from the mould their void ratio increases to 0.26. The void ratio increased slightly to around 0.33 due to saturation. The final void ratios of the dry pressed samples (prior to consolidation) are much higher than that of the slurried sample compressed isotropically to a similar minimum void ratio illustrated in Figure 5.13.

This higher void ratio is believed to be primarily due to yielding that occurs during the one-dimensional unloading (Fig. 5.15a). As the axial stress is reduced after forming the samples in the mould, a unique structure with well defined shear planes is believed to be created. Consideration of the stress path followed in the mould suggests that the sample may reach a state of passive yield and failure. Upon unloading, the soil initially responds elastically and only small changes in void ratio occur. Eventually, the soil will reach a

limiting stress state and the soil will yield and expand as the soil heads towards a critical state (Fig. 5.15b).

The significant increase in the void ratio measured after removing the samples from the mould is consistent with this interpretation. However, there was no visual evidence of failure or preferential shear planes as following extraction from the mould the samples were still well compacted and apparently stiff and strong.

The difference in the final void ratios of the dry pressed and slurry specimens despite their compression to a similar void ratio suggests that the dry press specimens are

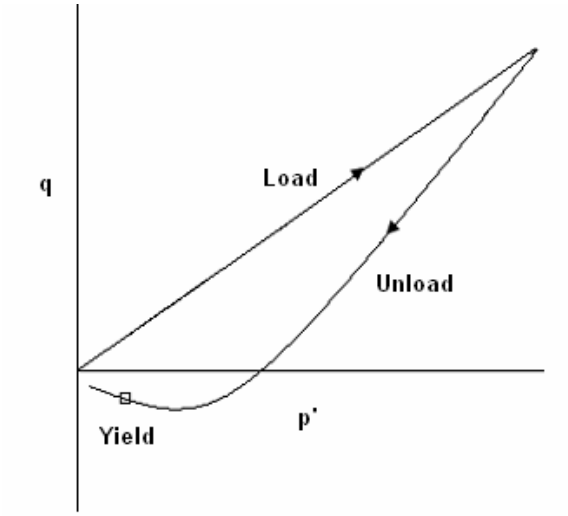

(a)

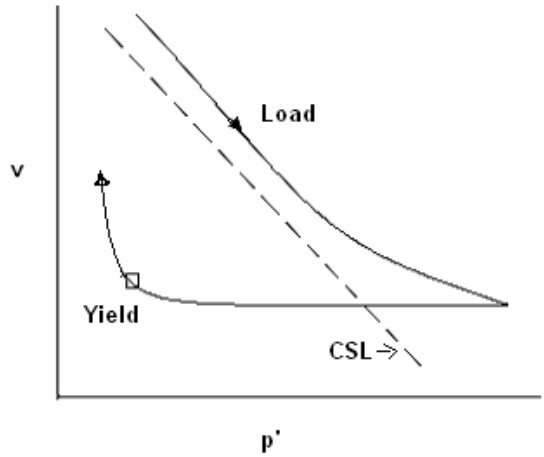

(b)

Figure 5. 15 Schematic responses of stress (a) and specific volume (b) during preparation of the dry press samples

more compressible than the isotropically overconsolidated specimens that have experienced a maximum pre-consolidation stress of 60 *MPa*. Extrapolation of the reloading response of the dry press specimens (Fig. 5.14a) to the *INCL* indicates a previous maximum stress of about 30*MPa*, which agrees with the pressure applied when forming the specimens.

This change in behaviour is believed to be due to the loading history having created a heterogeneous material with highly sheared bands of low density surrounding "intact" high density material, and that during isotropic compression the response is dominated by the material in these highly sheared bands. It can be shown that the compression response of the dry press specimens can be predicted (Appendix 5.1) if it is assumed that the specimens are heterogeneous with some of the material fully softened and the remainder intact with a low void ratio The influence of this imposed structure will be discussed in more detail later in this chapter.

§5.4.3.2 **Shearing responses of reconstituted specimens**

§5.4.3.3 **Normally consolidated specimens**

In order to study the behaviour of the reconstituted material, normally consolidated specimens were subjected to standard drained and undrained triaxial tests. Results for two representative specimens with confining stresses of 400 *kPa* and 1000 *kPa* are shown in Figure 5.16.

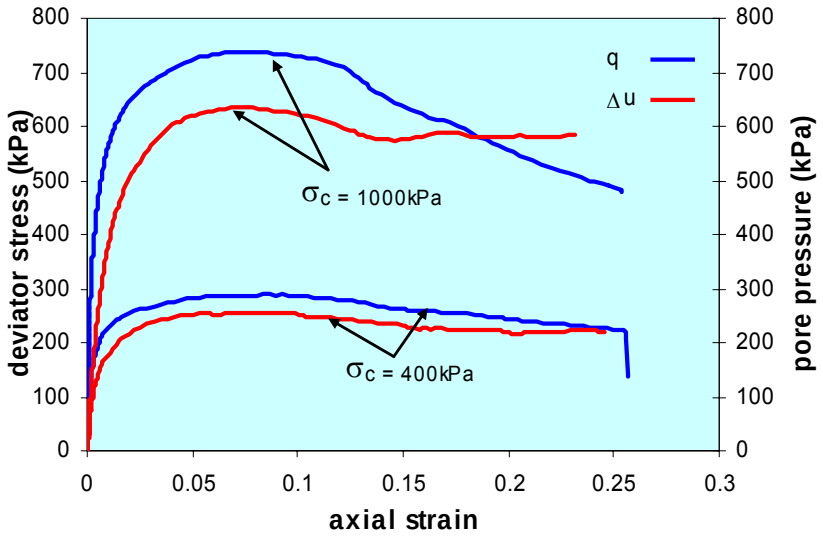

Figure 5.16 Stress, strain responses of normally Consolidated specimens

The figure shows the deviator stress, axial strain and the corresponding pore pressure responses. It can be seen from the graph that the stress-strain curve exhibits distinct peak strengths of 300 *kPa* and 750 *kPa* respectively. These defined strengths are not normally expected of normally consolidated soil. The failure mode of the normally consolidated undrained series (*NCU*) was associated with a strain softening behaviour and more non-uniform deformation. The shear plane occurred at an axial strain of approximately 8% (Appendix 5A). It is believed that the specimens are approaching a critical state at the peak, and that the subsequent reduction in strength is related to non-uniform deformation associated with the pronounced shear plane. The significance of the shear plane for these normally consolidated specimens is believed to be higher than usual because of the relatively low void ratio and hence high stiffness of these specimens. When normalised by the effective confining pressure at the start of shearing, p'_c, all the normally consolidated specimens showed similar behaviour (Figure 5.17).

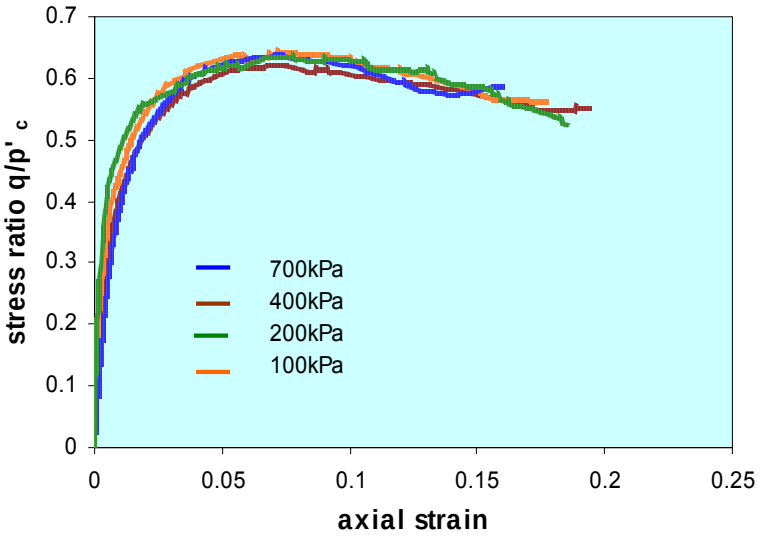

Figure 5.17 Normalised undrained stress-strain responses of NC slurry specimens

The effective stress paths from drained and undrained tests on isotropically normally consolidated samples to a range of confining pressures from 100 *kPa* to 1000 *kPa* are plotted in a plot of deviator stress, q (= σ'_1- σ'_3) versus mean effective stress, p' (= (σ'_1 + 2 σ'_3) / 3). For these samples, which have experienced a maximum effective stress of 1 *MPa* (Figure 5.18), a critical state line (*CSL*) can be defined given by M = 1.14 and a corresponding effective friction angle of ϕ' = 28.5°.

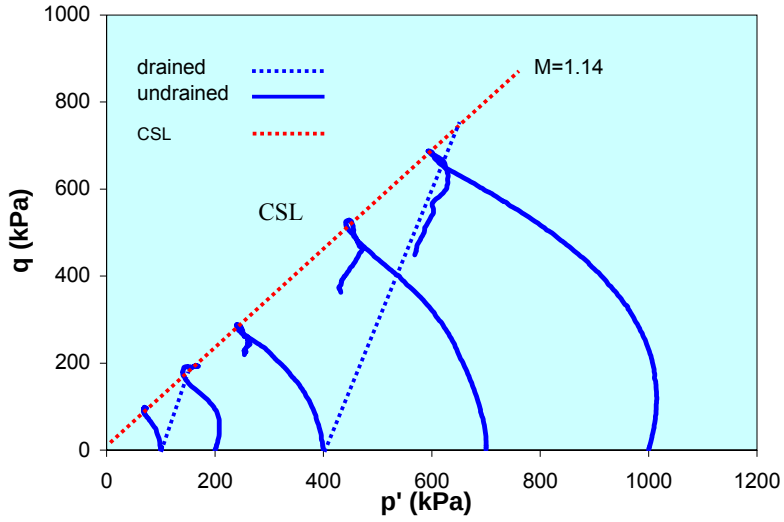

Figure 5.18 Effective stress-path of normally consolidated specimens at low pressure (slurry specimens)

With selection of failure points close to reaching a critical state (Table 5.2), it can be seen in Figure 5.19 that the critical state line (*CSL*) can be drawn nearly parallel to the *INCL*.

Table 5.2 Strength data showing q'_f, p'_f obtained from reconstituted slurry specimens at different pre-consolidation stress

Confining pressure(kPa)	1000	700	400	200	100
p'_f **(kPa)**	608	455	251	152	73
q_f **(kPa)**	674	514	272	191	96
ϕ **(degrees)**	28.8	30.1	31.3	34	35.8

The specimens which were highly compressed to a maximum effective confining stress of 60 *MPa* and sheared to failure under drained conditions (Figure 5.20) showed a different behaviour, as demonstrated by a low 0.67 value of *M* and a subsequent low effective friction angle of 16°.

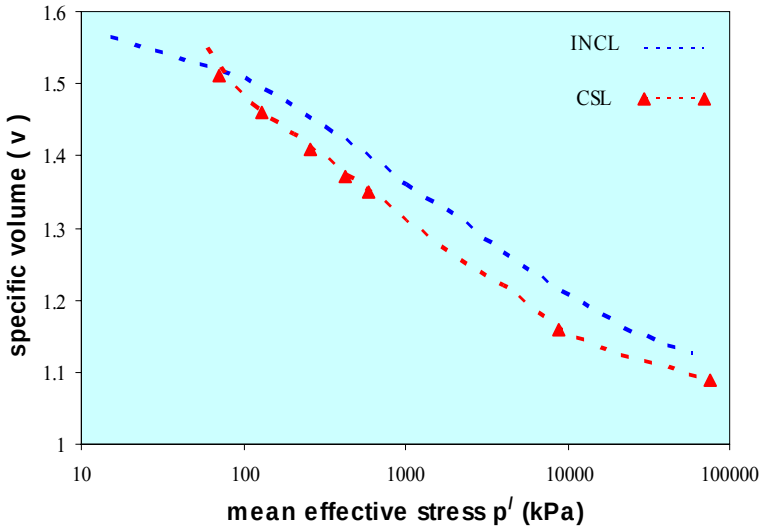

Figure 5.19 Normal consolidation and failure states of

reconstituted specimens

This different behaviour was unexpected for normally consolidated specimens as they were expected to behave similarly to other normally consolidated specimens once allowance was made for differences in confining stress level (e.g. Atkinson and Bransby, 1978). For the material that has experienced a maximum effective stress of 6 *MPa*, Figure 5.20 demonstrates a behaviour that is consistent with the assumptions of critical state soil mechanics and of the specimens subjected to < 1*MPa*. The behaviour of the normally consolidated shale was further investigated by examining the relationship between the normalised deviator stresses and the axial strains for specimens tested in a drained condition at different effective confining stresses (Fig. 5.21).

The figure demonstrates that similar responses are obtained for specimens tested at effective confining stresses of 0.4 and 6 *MPa*. It can also be seen that the response of the specimen with $p'_c = 60$ *MPa* lies significantly below the curves of the specimens that have experienced a maximum stress of ≤ 6 *MPa*. Both the final strength and the normalised stiffness are lower for the highly compressed specimen. When the highly compressed specimen reached a confining stress of 60 *MPa,* the void ratio was about 0.15 (Section 5.4.3). With such low void ratios it can be expected that the potential for

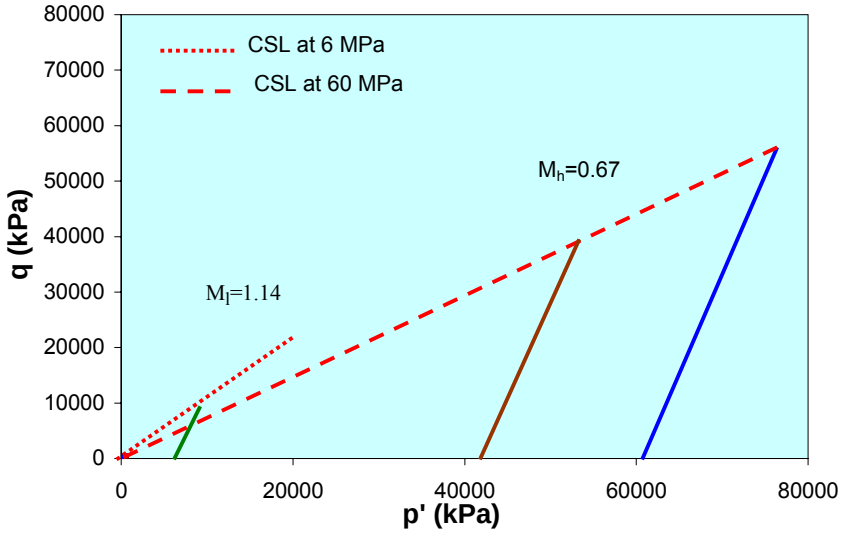

Figure 5.20 Strength envelopes of low (M_l) and high (M_h) pressure test series (slurry specimens at drained condition)

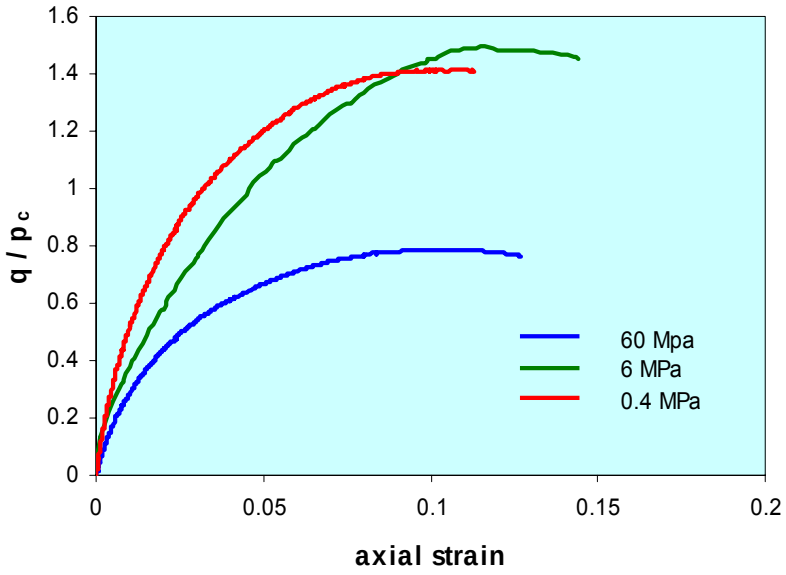

Figure 5.21 Responses from normally consolidated drained tests (slurry specimens)

further volume change (Fig. 5.22) is reduced as is indicated by the difference in volume strain with stress level.

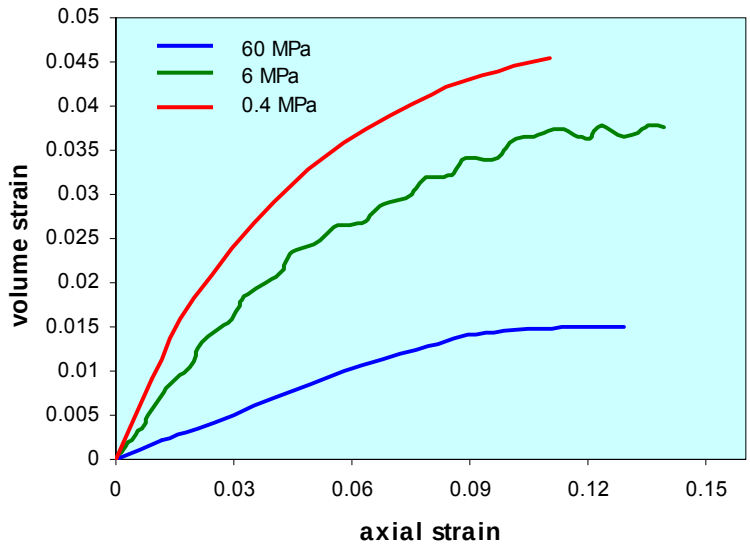

Figure 5.22 Influence of effective consolidation stresses
on specimens in a drained condition

The reduction in volume strain with stress level is consistent with the existence of parallel *INCL* and *CSL* lines in v : ln p'. This would predict volume strains of 0.045, 0.035, and 0.015 at stresses of 400 *kPa*, 6 *MPa*, and 60 *MPa* respectively. It is evident that ε_v for 60 *MPa* is consistent with the other lower stress levels as it is reflected from the differences in specific volumes at start of shearing. It has also been noted that the tendency for volume expansion on unloading is reduced when $p'_c = 60\ MPa$.

§5.4.3.4 **Overconsolidated specimens**

A series of standard drained (*CID*) and undrained (*CIU*) triaxial tests on slurry and dry pressed specimens were performed to investigate the effects of over-consolidation ratio (*OCR*). In order to examine the relationship between over-consolidation ratio and the behaviour of the material, the normalised effective stress paths, shown in Figure 5.23 are presented. The figure shows the outcomes of standard undrained tests

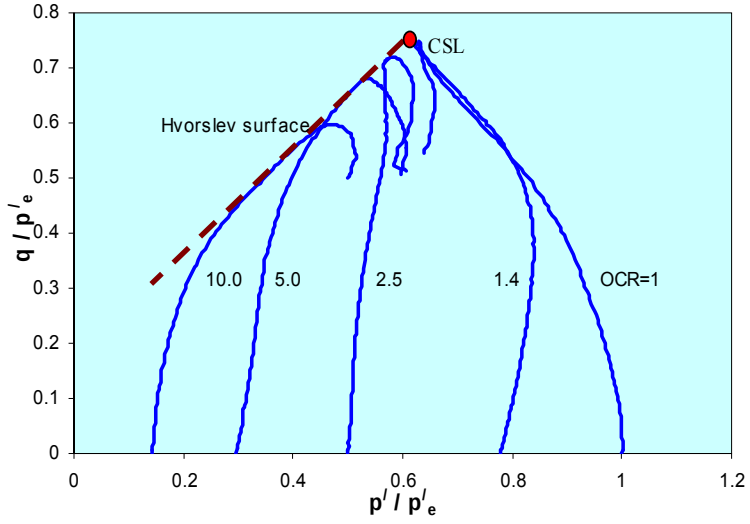

Figure 5.23 Normalised responses for specimens with
a maximum stress = 1 *MPa* (slurry specimens)

performed on slurry specimens with *OCR* up to 10 with effective confining stresses of ≤ 1000 *kPa*. The triaxial tests revealed a stress-strain strength behaviour that was consistent with many other reconstituted materials reported in the literature (Kato, 2000).

The effective stress paths of these tests have been normalized by p'_e, the pressure on the *INCL* at the same specific volume. They show a well defined Hvorslev failure surface culminating in a critical state with a friction angle of 28.5°.

Typical stress-strain and pore pressure response curves for an over-consolidated specimen prepared from a slurry are shown in Figure 5.24. The figure shows curves that are typical of over-consolidated clays (e.g. Atkinson & Bransby, 1978) in that the peak deviator stresses are greater than for normally consolidated samples at the same confining pressure, and negative pore pressures are generated during shearing. A similar typical response is also shown for a specimen prepared by the dry press method (Fig. 5.25).

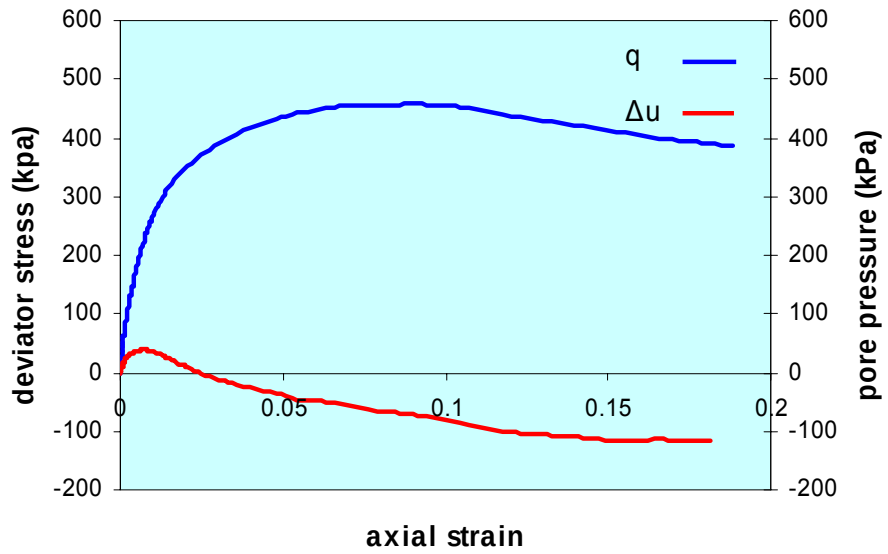

Figure 5.24 Stress-strain response of OC slurry specimen in a CIU test, OCR=10, $p'_c = 100\ kPa$ and $p'_{max} = 1 MPa$

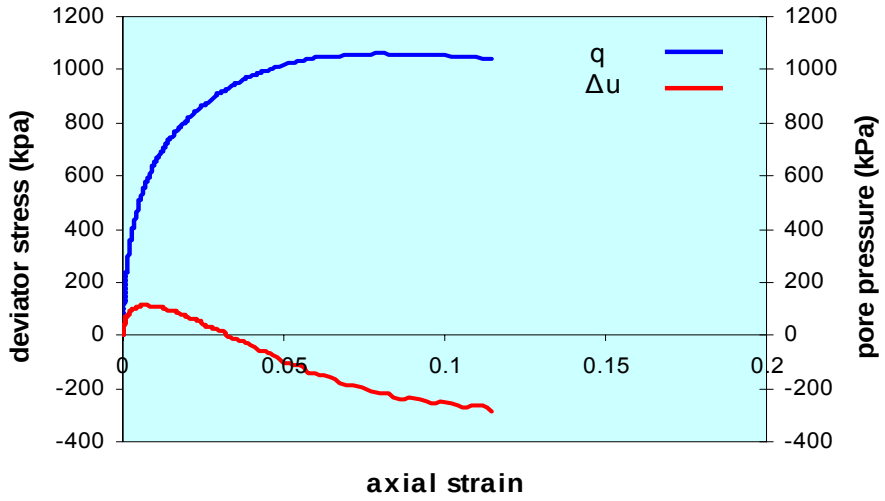

Figure 5.25 Stress-strain responses of OC dry pressed specimens in CIU tests, apparent OCR=10, $p'_c = 400\ kPa$

For the dry pressed specimens, the apparent *OCR* has been based on the specific volume and the compression line determined earlier from the isotropic compression response of the slurried specimens. This value of *OCR* that based on a maximum stress of 4000 kPa is much lower than the value of the *OCR*=30 that has been estimated from the ratio of past maximum under which the dry specimens were formed to current effective vertical stress.

The generated negative pore pressures in both figures are due to suppressed dilation as the specimens head towards failure. This was further investigated by examining the influence of the effective stress on the volumetric strains measured in drained tests of specimens at different *OCR* values (Fig. 5.26).

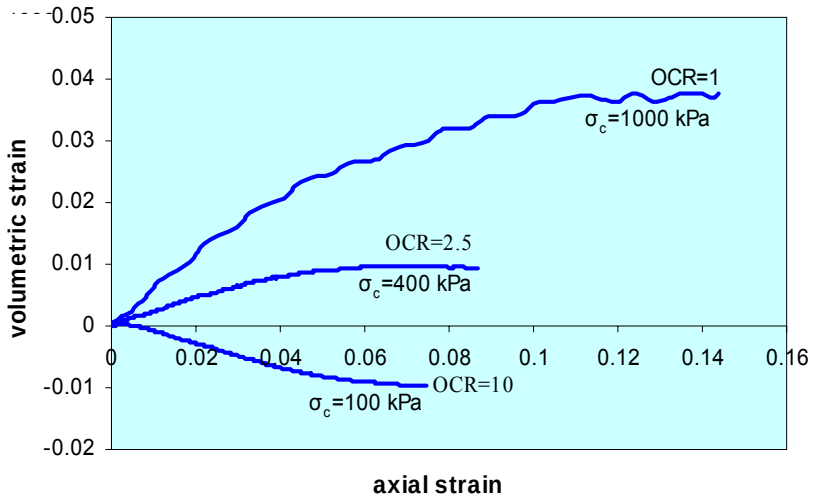

Figure 5.26 Dilation in specimens at low pressure in CID tests (slurry specimens)

Figure 5.26 shows the trend of decreasing compressive / increasing expansive strains as *OCR* increases, reported in many other studies (Atkinson and Bransby, 1978). A conventional interpretation of results from these graphs is based on their state in v, ln p' space (Fig. 5.13). This would indicate the specimens shown in Figures 5.24 and 5.25 have similar apparent over-consolidation ratios (*OCR*s) and the trends are similar. However, it should be noted that the *OCR* of the dry pressed specimen was based on their specific volume and $\kappa = 0.025$ while the *OCR* of the slurry specimen was based on a maximum pressure of 1000 *kPa*. The similarity in the trend occurred despite the maximum pressure of 30 *MPa* that the dry pressed specimen had been subjected to during preparation. However, the difference between the slurried and dry pressed specimens was evident from the difference in the strength and pore pressure of the two specimens. This difference in behaviour is due to two reasons; one is the high pressure the other is the heterogenous structure mentioned previously. In order to investigate the effect of the high

stress further, specimens from low and high pressure test series were plotted on one graph (Fig. 5.27) to show the effect of *OCR* on the behaviour of the reconstituted specimens.

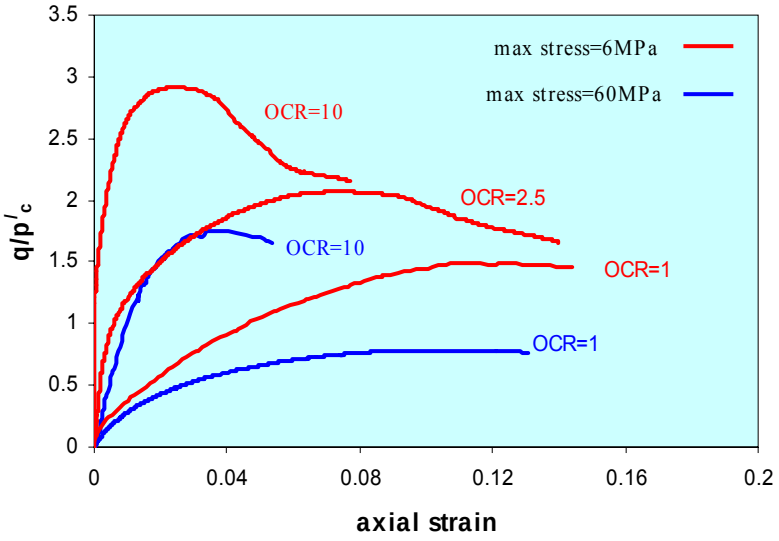

Figure 5.27 Influence of OCR on stress-strain responses in drained conditions (slurry specimens)

The figure shows deviator stress normalised by the effective consolidation stress, p'_c at the start of shearing. It has been shown that the normalised response of a specimen with p'_c = 6 *MPa* was similar to that at lower stresses. It is therefore believed that for maximum consolidation stresses of up to 6 *MPa* the normalised responses for a given *OCR* are unique, as reported in numerous studies on reconstituted clay (Kato, 2000; Burland, et al., 1996; Atkinson and Bransby, 1978).

The normalised responses of the specimens that have been compressed with a maximum stress of 60 *MPa* all lie significantly below the curves of the same *OCR* where the specimens had experienced a maximum stress of 6 *MPa*. It can also be observed that the final strength as well as the normalised stiffness are lower for specimens subjected to 60 *MPa*. Figure 5.28 shows that the volume strains for specimens with p'_c = 60 *MPa* are less than for specimen with p'_c = 1 *MPa*. As discussed above the reduction in ε_v is largely due to the low void ratio for the *NC* soil. It may also be noticed that the tendency for

volume expansion is greatly reduced when *OCR*=10 and the maximum effective confining stress $p_c' = 60\ MPa$.

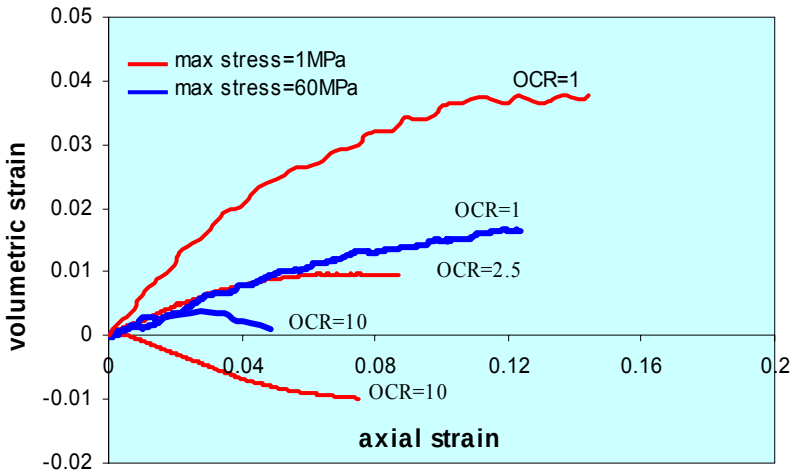

Figure 5.28 Influence of OCR and pre-consolidation stress on volumetric strain responses

The stress-strain and pore pressure response curves for overconsolidated specimens (Section 5.4.4.1) show that the peak deviator stresses are greater than for *NC* specimens at the same confining pressure and that negative pore pressures are generated during shearing. From these results, the influence of structure on the dry pressed specimen could be investigated by comparison between a slurry specimen and
a dry pressed one. Responses with different *OCRs* are plotted in a normalised plot in Figure 5.29. The dry pressed specimen with *OCR* = 6 (based on *v*, *INCL*) attains a much lower normalised deviator stresses than the slurry specimen with *OCR* = 10. However, the maximum pressure applied in forming the dry specimen was much higher than suggested by its specific volume, and an *OCR* range from 30 to 75 would be predicted based on the maximum stress. The lower normalised stress would indicate an *OCR* < 6, so the responses are clearly not consistent with a conventional interpretation based on the specimens states in the *v*: *ln p'* space.

It is believed that yielding on unloading has led to the development of softened zones (Appendix 5.A) within the stiff soil, and has produced a heterogeneous soil structure.

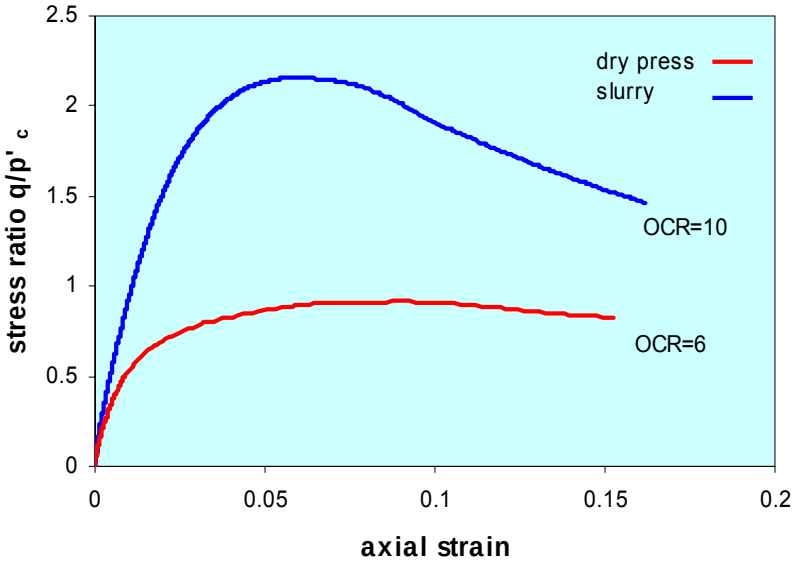

Figure 5.29 Normalised deviator stress of dry pressed and slurry forms in drained conditions

This soil structure may be associated with a different compression line as suggested by Cotecchia and Chandler (2000). They argued that different structures would result in different compression lines, however, they also showed that after appropriate normalisation similar patterns of behaviour were observed irrespective of the structure. This does not agree with the results from the dry pressed samples, which do not appear to be able to be normalised to give patterns of behaviour similar to other reconstituted soils. Another possibility is that a unique structure with well defined shear planes is responsible for the abnormal behaviour of the dry pressed specimens.

Support for this proposition is provided by the observed patterns of failure of the two different forms of reconstituted soils with the same *OCR* (Figure 5.30). The figure shows clear rupture planes for the low pressure slurry specimens, while the failure of dry pressed soil was associated with barrelling of the specimens. This barrelling is believed to be a result of developing a network of shear bands produced after removing the sample from the mould. In addition to the uniform deformation and absence of evidence of preferential shear planes, the greater compressibility of the specimen despite the lower void ratio and greater pre-consolidation stress, may also explain the insignificant change

in the volume strains developed in drained tests as the confining effective stresses increase (Fig.5.31).

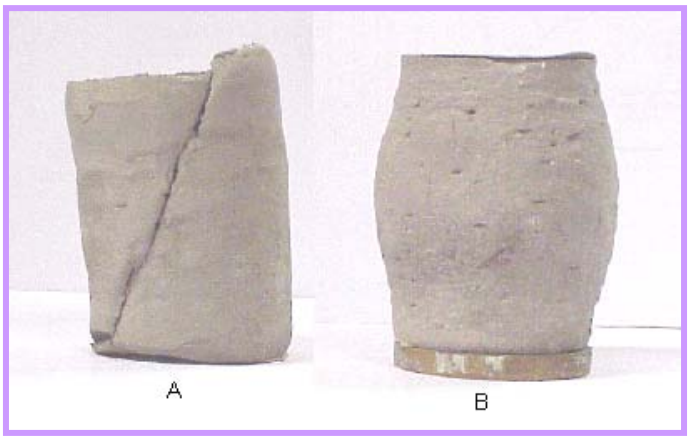

Figure 5.30 Different failure modes for slurry (A) and dry pressed (B) specimens of same OCRs

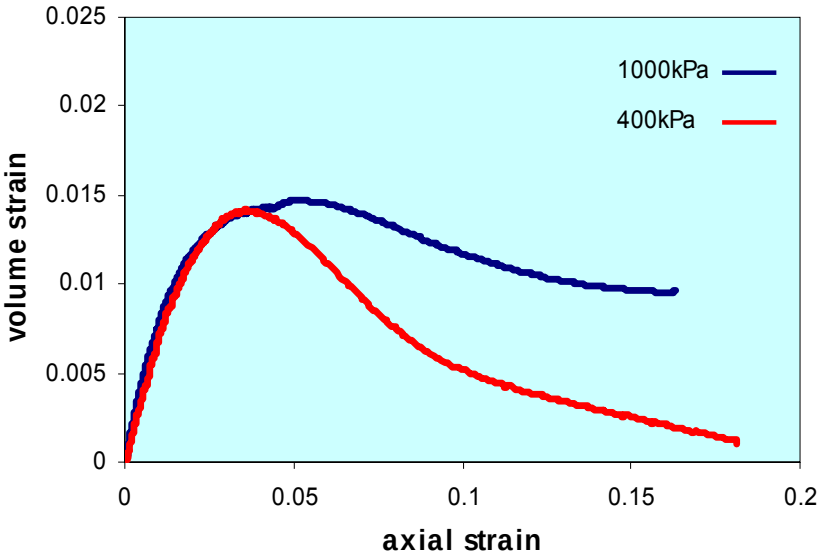

Figure 5.31 Influence of specimens compressibility on the volumetric strains of the dry pressed specimens at different confining stresses

§5.4.4 **Critical state in the context of the results**

The relevance of the critical state concept to the shear behaviour of the specimens formed from slurry and of those formed by dry pressing becomes apparent by examining the variation of the state paths for the specimens in normalised p' : q' : v space. The undrained effective stress paths of these specimens are plotted in the q' : p' plane in Figure 5.32.

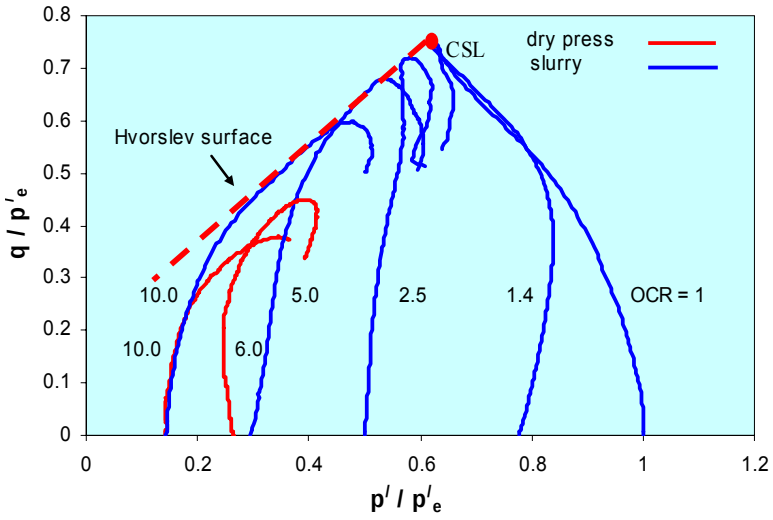

Figure 5.32 Normalised effective stress paths

This shows the normalised effective stress paths for tests with $p'_c < 6$ *MPa* performed at different stress levels. The plot can also be used as an effective method of examining the relationship between *OCR* and the behaviour of the material.

The figure demonstrates results for specimens formed from slurry and by the dry pressed method. Alongside each state path, the relevant value of *OCR* is shown. For slurry specimens, only typical paths are presented for any given *OCR* since many tests were duplicate tests. The stresses have been made dimensionless by dividing the stresses q' and p', by the relevant value of the equivalent pressure p'_e, the mean normal effective stress on the isotropic normal consolidation line at the current specific volume. The

values of λ and N determined from the normal consolidation line (Fig. 5.13) have been used to determine the parameter p'_e, the equivalent pressure, at any specific volume. The parameter has been calculated from equations (5.16 and 5.17) which describe the *INCL* and expressed as

$$p'_e = exp[(N-v)/\lambda] \qquad (5.18)$$

As discussed previously the critical state line is reduced to a single unique critical state point indicated by *CSL*. It can also be noticed that the normalised effective stress paths for all slurry specimens are typical of clay behaviour (e.g. Loudon, 1967; Atkinson & Bransby, 1978). The overconsolidated specimens attain higher value of stress ratio than the critical state. In this normalised plot, a Hvorslev surface can be defined as the locus of the peak strengths of the overconsolidated specimens.

The overconsolidated dry pressed specimens failed on attaining the critical state stress ratio below the Hvorslev surface found for the slurry specimens. Their intermediate behaviour is believed to be a consequence of their heterogeneity. This was evident during shearing where the dry pressed specimens reached an ultimate frictional strength identical to the specimens that have only been lightly compressed (e.g. M= 1.14, $\phi' = 28.5^o$), while showing some expansive volumetric strains.

As stated previously, very significant differences in the normalised responses are indicated for all *OCR*s when the maximum confining stress is increased to 60 *MPa*. These variations were associated with a reduction in normalised stiffness and strength. The different behaviour of the highly compressed material (Fig. 5.33) can be seen from the normalised failure envelope, shown by the broken line, that lies significantly below the *CSL* and *Hvorslev surface* for specimens subjected to a maximum stress of 1 *MPa*.

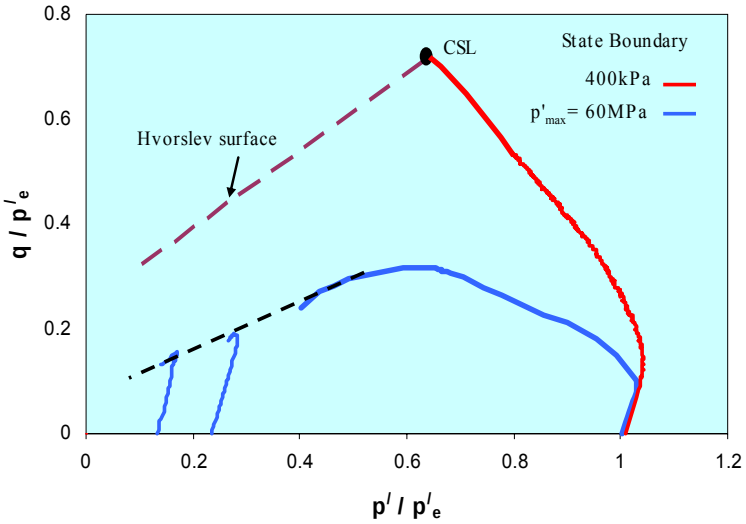

Figure 5.33 State boundary surface of reconstituted shale at low and high stress level

The difference in the envelopes at different stress levels reflects clearly the different shape of the sections at constant *e*, and of the state boundary surface (*SBS*). Although the response is qualitatively similar when compressed to 60 *MPa*, the normalised responses lie significantly below Hvorslev surface obtained at lower stress levels and higher void ratio. The ultimate friction angle has been reduced to only 17°, less than the critical state friction angle determined at lower stress level (Section 5.4.4.3). The plot also confirms the influence of increasing *p*' on the significant changes in the shape of the *SBS*.

For low pre-consolidation stresses, the material behaves as would be expected from the concepts of critical state soil mechanics, but the patterns of behaviour of the specimens from the high pressure test series are not consistent with the existence of a unique critical state line which would have required much greater dilation particularly
for specimens with higher *OCR* values. Based on these observations, one can also suggest that the concept of an *OCR* as a means of normalising the results has little use for analysing specimens from the high pressure test series.

§5.4.5 **Stiffness of reconstituted shale**

The deformation of Bringelly shale has been investigated using data from drained and undrained tests on reconstituted specimens. All tests were performed to failure and stresses and strains were determined from an external load cell and *LVDT*. Data from external measurements were obtained from the following tests:

(i) *NC* drained with maximum consolidation stresses ranging from 0.4 to 60 *MP*a,
(ii) *OC* undrained with a maximum effective confining stresses = 1 *MP*a, and
(iii) *OC* drained with a maximum preconsolidation stress = 60 *MP*a.

In order to assess the possible errors in stiffness resulting from external measurements and the spherical seat, one test was performed on a 50 *mm* diameter specimen using bender elements. In this test, two bender elements were embedded in the triaxial platens to estimate the shear modulus more directly.

a. using bender element

For one of the reconstituted specimens, an isotropically consolidated drained triaxial test was conducted in which bender elements were used to measure shear wave velocity and Hall Effect Transducers (*HET*s) to directly measure sample deformations. The triaxial cell and its attached devices (Fig. 5.34), including bender elements were used to determine the shear wave velocity and hence shear modulus at very small strains. Two bender elements were used (Fig. 5.35), one causes the waves to propagate through the soil and the second to detect and convert the mechanical waves to an electrical pulse. By measuring the time delay between the applied and received pulses a shear wave velocity can be calculated knowing the distance between the bender elements. The shear modulus can then be determined using the following expression:

$$G = \rho v_s^2 \qquad (5.19)$$

where

G = shear modulus

ρ = bulk density

v_s =shear wave velocity = L/t

L =length between the tips of the bender elements

t = time delay

Details of equipment, procedure involved, and the principle of using bender elements are given by Mohsin et al. (2004). Figure 5.36 shows the relation between G_{max} and mean effective stress determined from the bender elements.

The direct measurement of G was obtained for a specimen consolidated to, and sheared at 400 *kPa* effective confining stress. Even though the test had to be terminated at p'= 400 *kPa*, it was possible to determine a relationship between p' and G for the normally consolidated soil as explained in the next section.

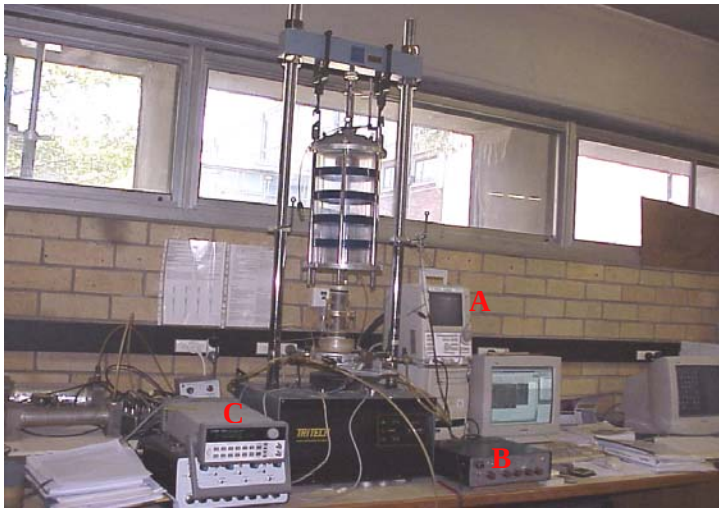

A: digital oscillator **B**: amplifier **C**: function generator

Figure 5.34 Devices used to measure shear modulus of reconstituted Bringelly shale

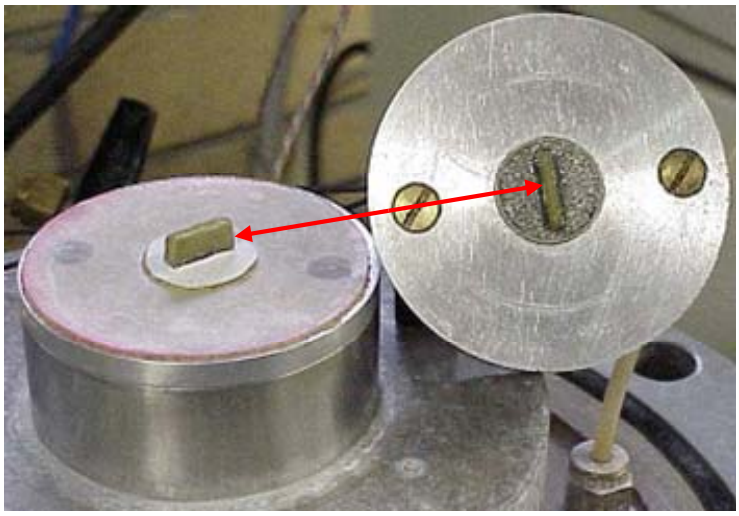

Figure 5.35 Bender elements (red arrows) attached to the end platens of the triaxial equipment

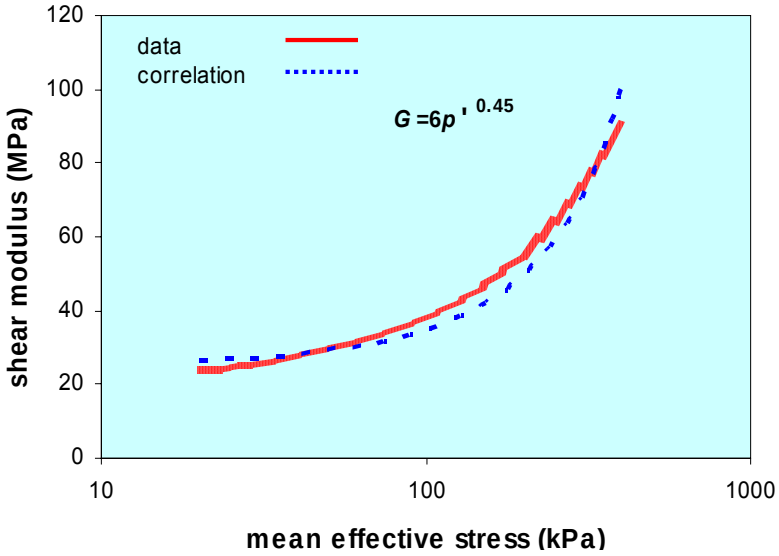

Figure 5.36 Influence of stress levels on the shear

modulus

Many authors have proposed correlations between p' and G or E such as Kulhawy (1975) who suggested a power law expression in the form

$$E = K' p_a \left(\frac{\sigma_3}{p_a} \right)^n \qquad (5.20)$$

where

E = Young's modulus
K'= modulus number
n = modulus exponent
σ_3 = confining pressure

p_a = atmospheric pressure in the same units as σ_3 , and E to ensure that K' and n are dimensionless numbers

In the current study, a plot of G from the bender elements versus p' shown in Figure 5.36 was used to examine the experimental data. The graph indicates that a large increase in shear modulus is associated with a smaller change in the mean effective stress particularly when p' exceeds 100 *kPa*. The variation shown in the figure is best described by the following equation:

$$G_{\max} = 6 p'^{0.45} \qquad (5.21)$$

where $G_{\max}$ is measured in *MPa*, and p' in *kPa*. Regression analysis shows that equation 5.21 correlates well with the data as demonstrated by the two curves in the figure.

b. using Hall Effect Transducers (*HET*s)

An indirect determination of the shear modulus was also calculated for the same specimen tested with the bender elements that was isotropically compressed to 400 *kPa* effective stress and then sheared drained. Based on data from the *HET*s, the stress-strain relationship and *Poisson's ratio* were determined. The following expression was used:

$$G = \frac{E'}{2(1+\nu')} \qquad (5.22)$$

Where

E' is the drained stiffness

ν' is the Poisson's ratio

For this specimen, a drained stiffness and a Poisson's ratio of 250 *MPa* and 0.35 were calculated respectively. Based on the above equation, a shear modulus of $\cong 93$ *MPa* was determined. This *G* value is consistent with the value of 90 *MPa* measured directly from the bender elements.

§5.4.5.1 **Responses to stiffness**

The stiffness of the reconstituted shale was also determined from external measurements during the triaxial tests. The influence of *OCR* on the variation of the secant stiffness in undrained and drained conditions is shown in Figures 5.37 and 5.38. In both figures the stiffness has been normalised by the effective consolidation stress and then plotted versus the axial strain. The first figure shows a clear trend in the variation of stiffness with strain level, the stiffness dropping to small values at large strains between 8% to 12% corresponding to failure. It also shows the influence of *OCR* on the variation of the undrained secant stiffness with axial strain, with increasing *OCR* resulting in increasing

normalised stiffness. However, the dry pressed specimens do not fit in with the trend for *OCR*. The normalised stiffness variation with strain is similar to that for the normally consolidated slurried specimens. It is clear that the dry press method of specimen preparation used to create the low porosity specimens has had a profound influence on the stress, strain, and strength response. This is further evidence that response of the dry pressed specimens is controlled by softened zones as postulated above.

The second figure (Fig. 5.38) shows the influence of confining stress on the drained stiffness of normally consolidated specimens for stresses from 0.4 to 60 *MPa*. Although not directly comparable with Figure 5.37 because of different drainage conditions, the two plots show similar values of normalised undrained and drained stiffness at low confining stress levels. The figure shows the large drop in normalised stiffness that occurs as the confining stress increase. However, Eq. 5.20 suggests that the elastic modulus E is proportional to the mean effective stress $p'^{0.45}$. When the maximum value of the E at very small strains is divided by the $p'^{0.45}$, it gives normalised values of 430, 550, and 480 at 0.4 *MPa*, 6, *MPa*, and 60 *MPa* respectively.

These values are close enough to bring the curves within a significantly small range of normalised stiffness and suggest that Eq. 5.21 is valid for reconstituted specimens over the stress range of 0.4 *MPa* to 60 *MPa*.

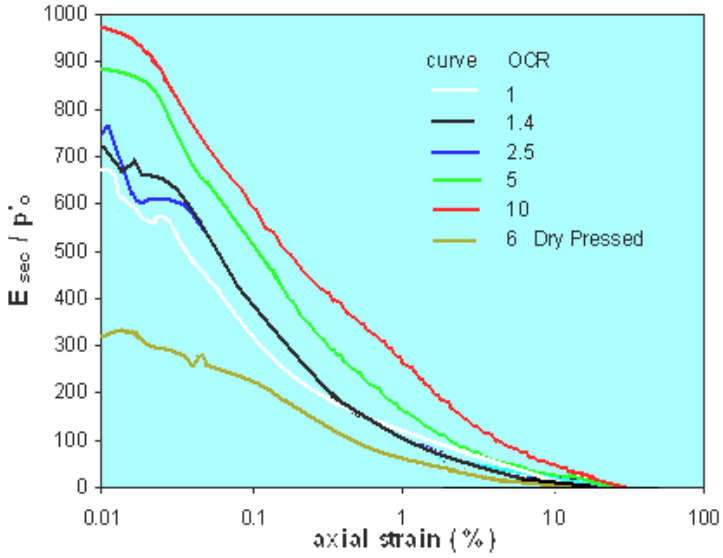

Figure 5.37 Variation of undrained secant modulus with the strain of reconstituted specimens

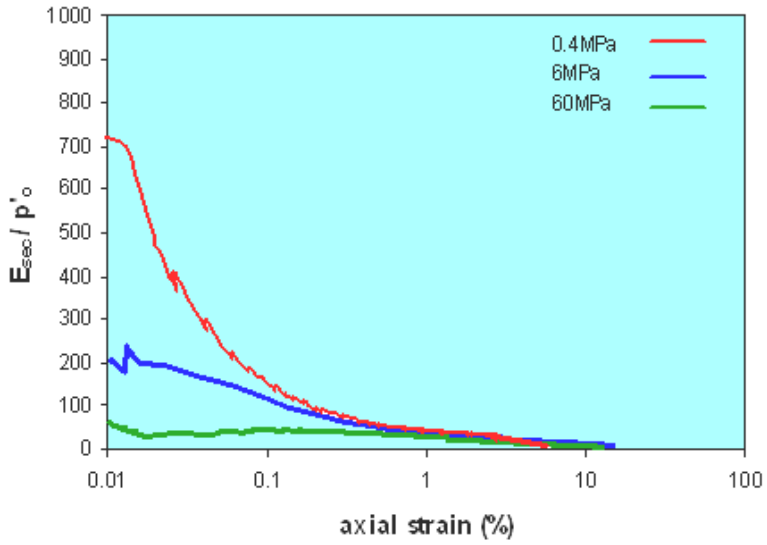

Figure 5.38 Drained secant modulus of NC specimens at low and high effective stresses

However, the influence of the maximum consolidation stress is more pronounced as shown by the reduced values of normalised drained stiffness of specimens subjected to a maximum stress of 60 *MPa* (Fig. 5.39).

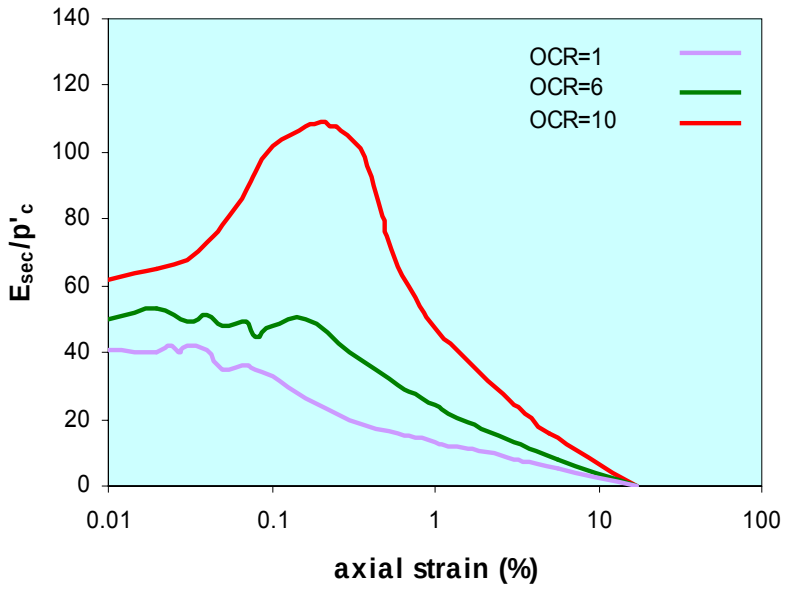

Figure 5.39 Variation in drained stiffness of OC specimens for specimens compressed to a maximum stress of 60 *MPa*

The figure shows the influence of *OCR* on the variation of the drained secant stiffness with axial strain, with increasing *OCR* resulting in increasing normalised stiffness. This trend is consistent with the trend for the undrained secant stiffness and confirm the similarity in the responses of the specimens regardless the stress level and the drainage condition of the material. However, it must be noted that the variation in the normalised stiffness is becoming insignificant when the material is compressed to a stress of 60 *MPa*.

§5.4.6 **Discussion**

Standard isotropic consolidated triaxial tests on reconstituted crushed shale specimens have involved loading, unloading, and reloading to a maximum effective confining stress of 60 *MPa*. The standard drained and undrained triaxial tests performed on saturated specimens with a maximum effective confining stress of *6 MPa* have revealed results that are consistent with many other reconstituted materials. The specimens reconstituted from a slurry showed expected patterns of behaviour for clayey soils.

A well defined normal consolidation line was established, for which similar normalised responses were obtained. The patterns of strength and stiffness variation with *OCR* were similar to other reconstituted clayey soils. However, the ultimate friction angle of 28.5^o determined from these tests was much greater than the friction angle of 17^o determined from tests on reconstituted specimens that were isotropically compressed to an effective pressure of 60 *MPa*. It is believed that the significant drop in the friction angle is due to the fabric associated with the low porosity, created by the high stress. At low porosity there must be locally a high degree of alignment of the plate-like clay particles. This could lead to sliding shear mechanisms assuming increasing importance. More investigations regarding the mechanism leading to reducing friction angle and strength will be discussed in Section 5.5.

Direct comparison of the test results obtained in this section with work carried out on other material was difficult since laboratory-induced high pre-consolidation stresses do not appear to have been reported for clayey soils. All the normalised effective stress paths of reconstituted slurry and dry press forms are presented in Figure 5.40. The plot shows that the behaviour of the normalised paths of the reconstituted specimens is greatly influenced by the level of effective confining stress. The responses of specimens with $p'_c = 60$ *MPa* fail to attain the Roscoe surface and to reach the *CSL* determined from tests with $p'_{max} < 6$ *MPa*. The figure also shows that the normalised state boundary surface of the highly compressed material lies below the surface for the material subjected to lower pre-consolidation stresses. The peak strengths of the highly compressed specimens define an envelope that is well below the Hvorslev surface that was previously defined from the tests with a maximum effective stress of 6 *MPa*.

The results for the dry pressed specimens do not appear to be explainable within conventional soil mechanics theories, as the responses show aspects of normally and over consolidated behaviour, that are not consistent with the widely accepted framework for reconstituted soil. This was evident from the failure envelope that shows the behaviour of

the material as intermediate between the behaviour of the highly compressed specimens and that of the low pressured ones, as illustrated in Figure 5.40.

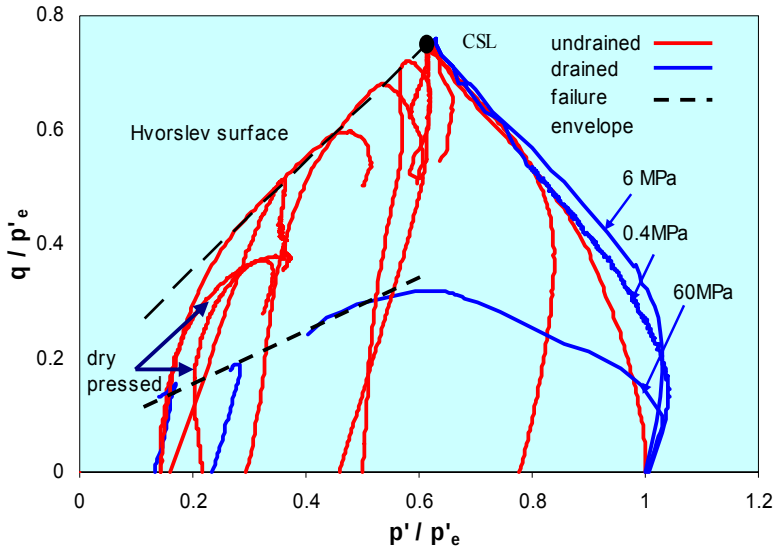

Figure 5.40 Normalised state boundary surfaces for different forms of specimens at different stress levels

This is believed to be a result of the heterogeneity created by the method of the specimen preparation whereby the specimens have experienced structural damage due to the high 1-D compression and unloading. The dry pressed specimens also have a shear stiffness similar to normally consolidated specimens. It is apparent that the use of *OCR* and other conventional means of normalising soil behaviour are not appropriate for the dry pressed specimens

§5.4.7 **Natural results**

§5.4.7.1 **Compression stress paths of natural shale**

One of the main focuses of this study was to investigate the strength and stiffness of the natural shale, particularly the influence of its low porosity and partial saturation.

In order to do so, it was necessary to find out how the Bringelly shale, which apparently has little cementation, can give *UCS* strengths of up to 50 *MPa* (Section 4.3.1). The influence of saturation on the behaviour of the natural material was thought to be important in influencing the mechanical behaviour. Because stiffness and strength of a material are important in geotechnical design, isotropic compression tests on natural specimens were performed. Triaxial tests were performed on natural shale in two states, the first was at the in-situ moisture content, and the second with the specimens saturated. The following sections will cover results for both unsaturated and saturated natural shale with special emphasis on the influence of saturation on the behaviour of the shale.

§5.4.7.2 **Unsaturated condition**

Drained triaxial compression tests were performed on specimens from the *KC* and *BC* sites. The specimens were sheared over a range of confining stress from 0 *kPa* to 6000 *kPa*. Typical stress-strain relations at different stresses for specimens at their in-situ water contents and degrees of saturation range between 53 to 70% are presented in Figure 5.41.

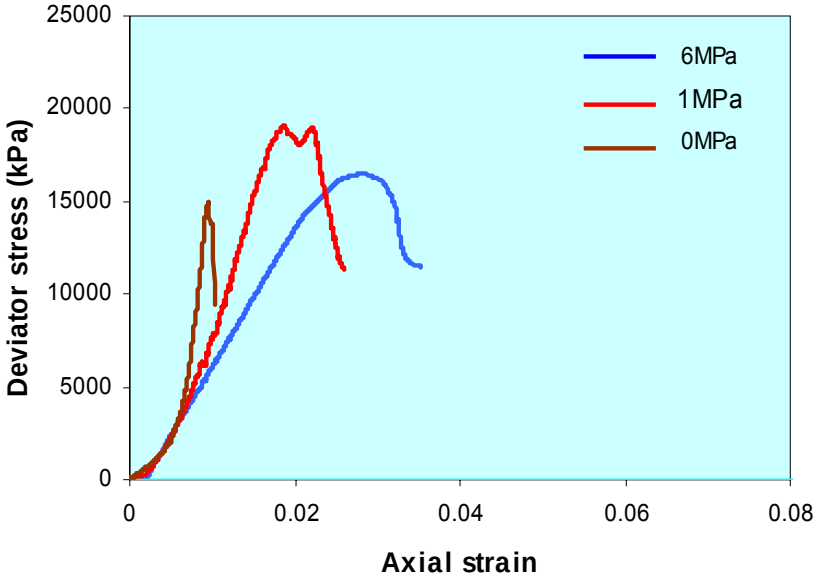

Figure 5.41 The influence of confining stresses on the behaviour of unsaturated natural shale

The Figure shows that the slight variation in the final strength is dependent of the variations in the confining stress over the range of stresses 0 – 6 *MPa*. For instance, at 6 *MPa* the peak strength approached 1700 *kPa* while 2000 *kPa* and 1500 *kPa* were the peak strengths at 1 *MPa* and 0 *MPa* respectively. It is believed that the influence of the confining stress on the behaviour of the materials is to be a result of the variation in their degree of saturation and the fabric of the material. However, it should be noted here that strength of the material is independent of its stiffness. The linearity of the stress-strain relationship can only be observed when the specimens reach a deviator stress of 3000 *kPa*. Below this stress, the initial stiffness of the specimens shows a non-linear and increasing trend. One possibility that could explain the non-linearity is that the stress applied to the specimen at the commencement of the test results in a closure of the internal micro-cracks of the specimen. Another possibility is that the re-arrangement of the weakly bonded particles in the material takes place as soon as the stress is applied to the material. This re-arrangement is a function of the applied stress. Another possibility is that external displacement measurements are affected by seating errors and misalignment of the ram with the top cap.

The initial stiffness of these tests appears to be similar and the data suggest that stiffness decreases with confining stress. This suggests some cementation is present in the shale as the absence of cement would show an increase in stiffness associated with an increase in the effective stress. From these results it appears that Bringelly shale is a “strong” rock with significant cementation.

§5.4.7.3 **Saturated condition**

Specimens were saturated under an effective stress of 600 *kPa*. As discussed in the previous chapter (Section 4.4.2) this stress was sufficient to prevent disintegration of the specimens, however, it was found to be associated with swelling strains. The responses of specimens during isotropic swelling and compression from saturation at 600 *kPa* are shown in Figure 5.42, together with the response of the reconstituted material. Comparison of the isotropic responses of the reconstituted material and the

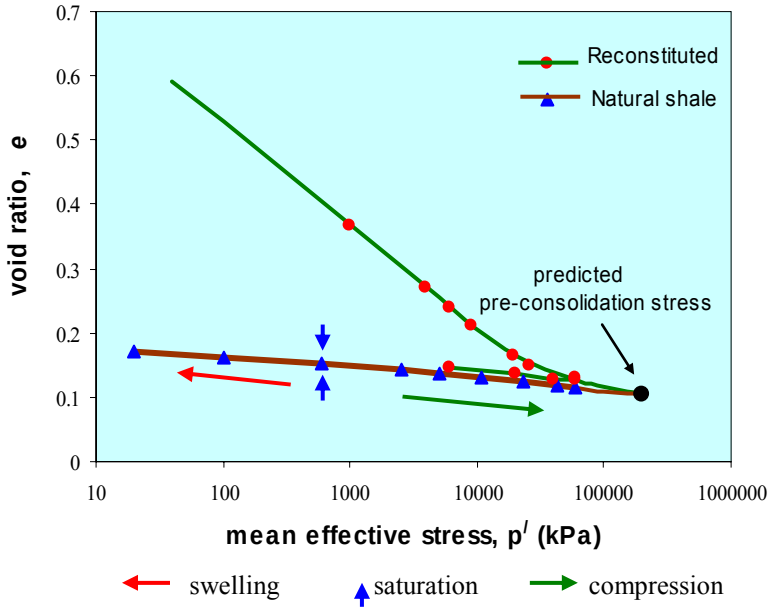

Figure 5.42 Isotropic compression response of natural and reconstituted material

natural shale indicate an effective confining stress of 60 *MPa* produces a void ratio of 0.15 and 0.10 for the reconstituted and natural shale respectively. These values are equivalent to the average porosity of ~10% previously measured for the natural shale (Section 4.2.2). As the shale appears to be only weakly cemented and not to have undergone significant diagenetic changes, the compression responses suggest that the natural shale has experienced a maximum effective stress of >60 *MPa*. The rate of reloading of the natural shale was 0.0012 *mm*/*min*. It is clear from the compression and swelling parts of the natural shale that the slope of the curve is increasing with increasing effective stress. It can be seen that the void ratio increases from 0.10 at a maximum effective stress of $p'_c = 60\ MPa$ to 0.18 at a minimum effective stress, $p'_c = 20\ kPa$.

Typical stress-strain curves of the natural material sheared over a range of effective confining stresses varying from a maximum of $p'_c = 60\ MPa$ to a minimum of 0.02 *MPa* are shown in Figure 5.43. The Figure shows that the higher the value of p'_c, the

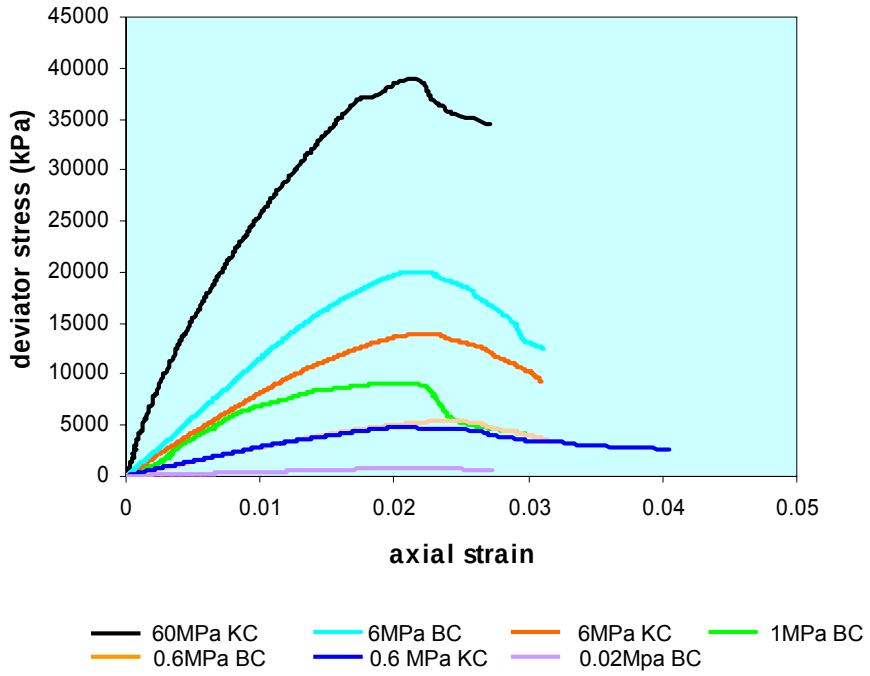

Figure 5.43 Drained stress-strain responses of saturated Bringelly shale in drained conditions at different effective confining stresses.

higher is the deviator stress as would be expected of a frictional material. It also shows that almost linear elastic responses are observed for deviator stresses up to 6 *MPa* in marked contrast to the responses of the unsaturated specimens. All specimens reached a peak (q) at an axial strain of about 2% and this was followed by a reduction in the deviator stress with further strain beyond the peak. It is interesting to note that after saturation the non-linear response is absent, suggesting that seating errors are not that significant as these should equally affect all tests on the natural core specimens.

To further investigate the behaviour of the saturated drained specimens, the deviator stress was normalised by the effective consolidation stress, p'_c at the start of shearing (Fig. 5.44). Inspection of the figure shows that the specimen sheared at the lowest effective confining stress of 20 *kPa* attains a much higher normalised deviator stress compared to those sheared at maximum $p'_c = 60$ *MPa*. The figure shows a similar trend to

the normalised response obtained previously (Fig.5.21) for reconstituted specimens. However, the maximum normalised stress value for the reconstituted

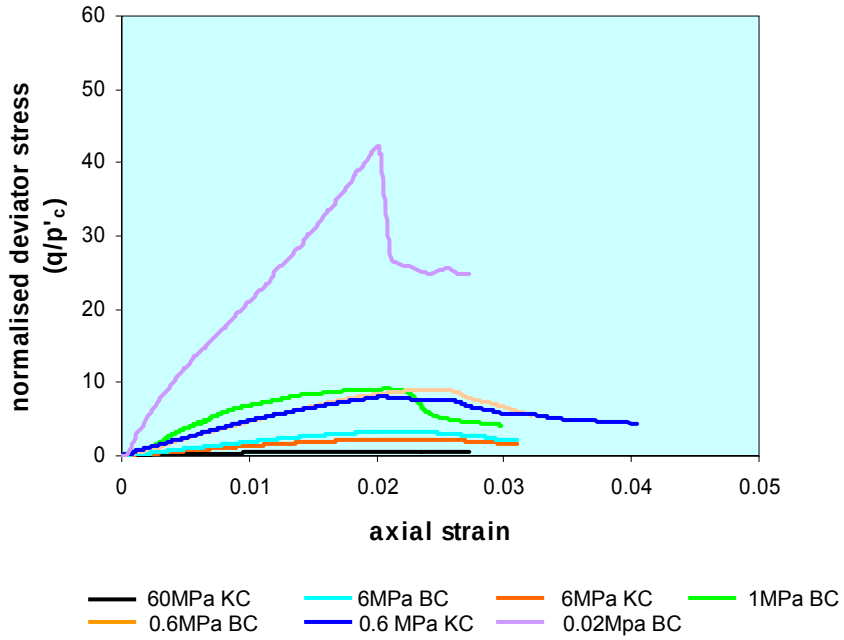

Figure 5.44 Normalised strength of saturated natural specimens

specimens is significantly lower than that for the natural shale particularly at effective stresses <.60 *MPa*. This reflects the influence of the structure and cementation in increasing the material strength and stiffness at stresses below the estimated maximum pre-consolidation stress of the natural shale. The plot also confirms that the preparation of the reconstituted specimens causes a significant loss of "structure" in the natural material.

At 60 *MPa*, a difference in behaviour is observed with the reconstituted specimens showing a less stiff behaviour than the natural shale. This is demonstrated in Figure 5.45 which shows the responses of the reconstituted and natural shale specimens at a consolidation stress of 60 *MPa*. The natural shale appears to be stiffer than the reconstituted one and a significant drop in the strength of the natural material is observed after the peak. This drop in the strength is believed to be due to the breakdown of "structure" in the natural shale. Also the peak for the natural shale occurs at smaller strain

while the reconstituted material shows a less pronounced peak occurring at a larger strain. The figure also shows no change in the normalised deviator stress after 4% axial strain. The similarity in the strength of the reconstituted

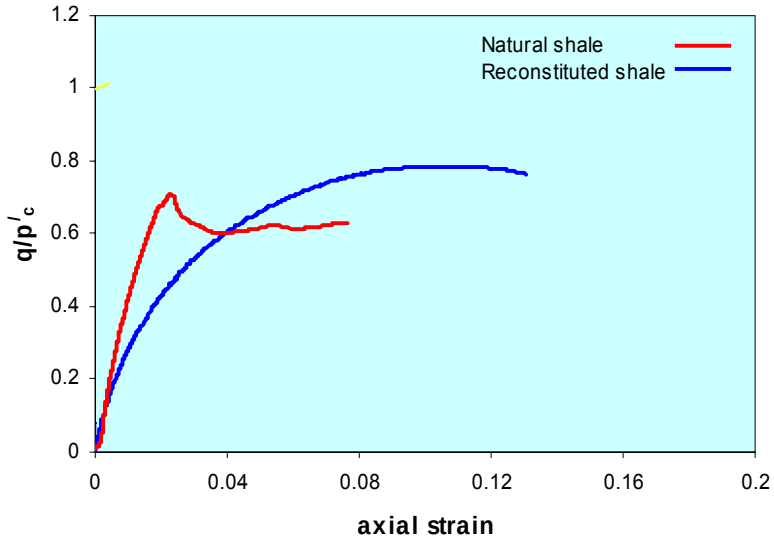

Figure 5.45 similar strength of natural and reconstituted material at 60 MPa confining stress

material, without any geologically induced structure or micro-cracks, and the natural shale suggests that the structure is not important in controlling the strength at 60 *MPa*.

Another possible reason for the difference in responses is that the natural shale is slightly overconsolidated at 60 *MPa*. The trend of the compression line of the reconstituted material and the reloading line of the natural shale appear to intersect at a mean effective stress > 100 *MPa*. The extrapolated lines and the suggested point of intersection are shown in Figure 5.42. The estimated pre-consolidation stress of p' = 200 *MPa* for the natural shale would indicate *OCR* of about 3 for natural shale sheared at p' = 60 *MPa* which could partly explain the greater stiffness and post-peak brittleness. However, the geological data (Chapter 2) suggest a maximum overburden stress of about 60 *MPa*. An apparent *OCR* may also develop due to creep and induration.

The influence of *OCR* on the failure mode of natural rock was investigated through examining the failure pattern of two specimens, one sheared at a confining stress of 60 *MPa* and the other at 20 *kPa*. The failure of the first was associated with a well defined failure mode with a distinct single rupture plane (Figure 5.46a), the second shows a shear plane that is less pronounced and demonstrated by small sheared bands and also by a circumferential enlargement at the base of the specimen (Fig. 5.46b).

a b

Figure 5.46 Typical failure mode and swelling demonstrated by natural shale at 60*MPa* (a) and 20 *kPa* (b)

This enlargement is believed to be a result of swelling due to the unloading from a high confining stress to a lower confining stress. However, the shearing and swelling patterns exhibited by the specimens explain part of the material behaviour which is consistent with the stress-strain responses observed previously for natural rocks sheared at different confining stresses.

§5.4.7.4 **Influence of stress and saturation on the failure of natural shale**

Tests were performed on specimens from *BC* and *KC* at effective confining stresses that varied from zero to 60 *MPa*. Typical outcomes of representative tests are presented in Figure 5.47. The Figure shows the failure points from these tests and indicates the very

dramatic effect of saturating the specimens on the strength. At a confining stress of 600 *kPa* the peak deviator stress drops from 15 *MPa* to 5 *MPa* as the material is saturated. The influence of saturation was more pronounced when the confining stress reduced to 20 *kPa*, the deviator stress dropping to 0.8 *MPa*, while the unsaturated shale strength was approximately 15 *MPa*. There are two possible factors

that may contribute to this large drop, one is the reduction in effective stress because of the removal of suctions leading to reduction in frictional strength, and the other is that the strains associated with saturation (Section 5.4.5.3) and effective stress reduction cause the material cementing the rock to break down.

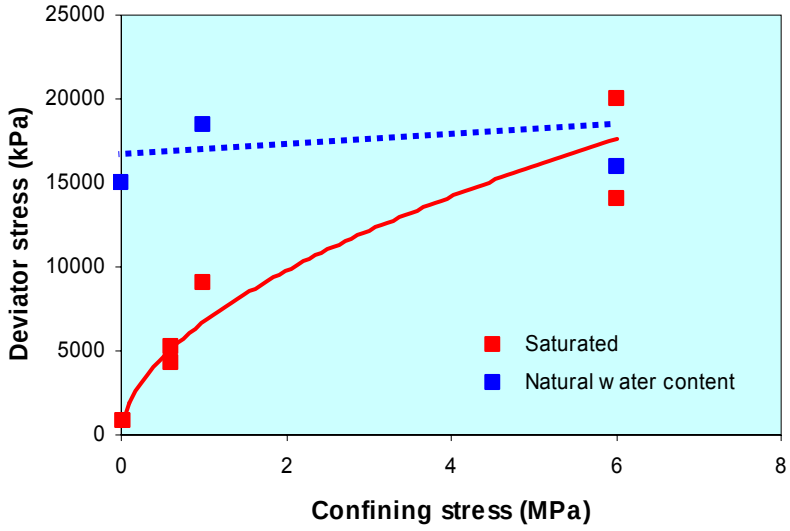

Figure 5.47 Influence of saturation on failure of the natural shale

To further investigate the above factors, a comparison of the deviator stress-strain response of saturated specimens, and specimens at the *in situ* moisture content is shown in Figure 5.48.

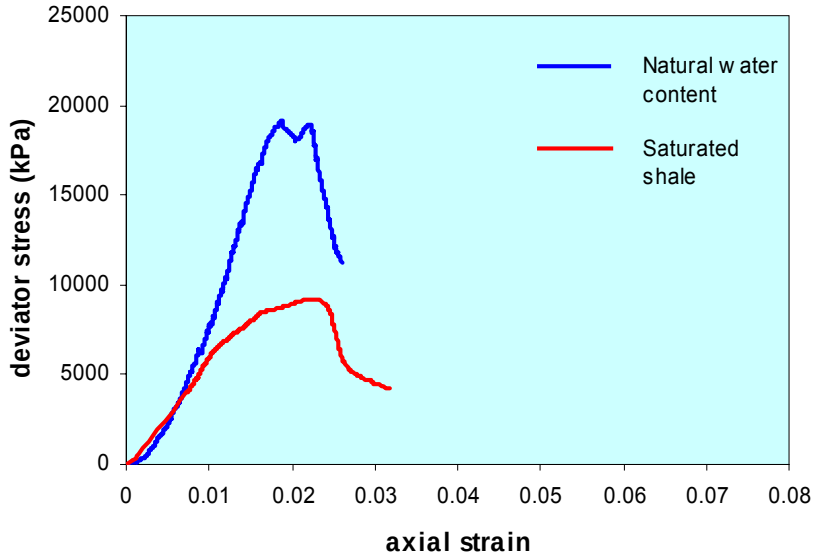

Figure 5.48a Stress-strain behaviour of unsaturated rocks at 1 *MPa* effective confining stress

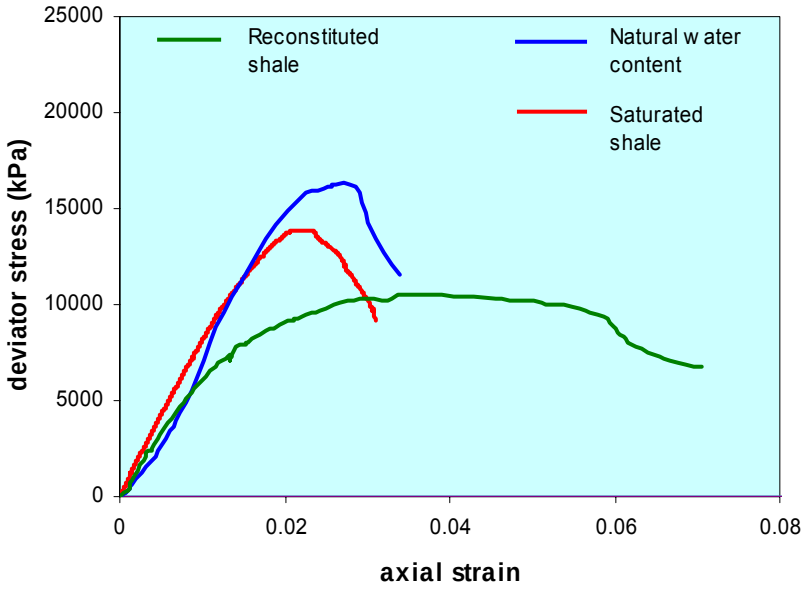

Figure 5.48b Effect of saturation on rocks at 6 *MPa* effective confining stress

For a confining stress of 1 *MPa* (Fig. 5.48a) the curves show that the initial stiffness is not greatly affected by the degree of saturation, but the strength is reduced significantly. This suggests some cementation is present in the shale as, if it was uncemented, the stiffness would be expected to vary with the confining stress, with the higher stresses in the unsaturated specimen giving rise to higher stiffness. The influence of saturation was also investigated through comparison with saturated reconstituted specimens at an effective confining stress, p_c' of 6 *MPa* (Fig. 5.48b). The figure shows a curve for reconstituted shale that had been pre-consolidated to 60 *MPa*, and two curves for the intact shale at its natural moisture content and when saturated.

As can be seen from the responses in Figure 5.48b, at 6 *MPa* the stiffness and strength of the intact shale are only slightly greater than the reconstituted material. This is a surprising result as standard rock mechanics procedures, discussed in Chapter 4, indicated the shale to be a strong rock. The two figures 5.48a,b, show that at lower confining stresses, the strength of the shale at its natural moisture content remains almost constant, as also shown by previous figures (e.g. Figs. 5.41 and 5.47). This suggests that any bonding present remains effective over the range of effective
stresses up to 6 *MPa*. An increase in the confining stress was accompanied by an increase in the stiffness by a factor of about 2 between effective confining stress of 0 and 6 *MPa*. One would expect a corresponding increase in the strength. It has been shown that cementation is relatively weak in this material, and that significant total suctions have been measured for the natural shale. It is thus believed that pore water suctions are largely responsible for the high strength and stiffness of the natural shale at low confining stresses. As confining stress increases, the suctions will reduce and the effective stress could remain approximately constant.

The influence of saturation on the reduction of the strength of the natural material is even more pronounced at lower confining stress (Fig. 5.49).

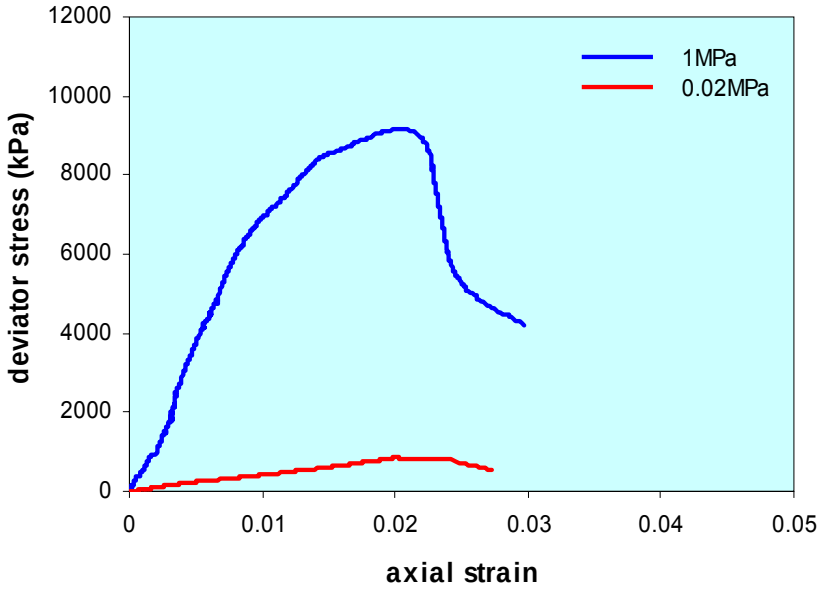

Figure 5.49 Influence of saturation at different confining stresses

The figure shows a reduction in the peak deviator stress by an order of magnitude as the confining stress drops from 1000 *kPa* to 20 *kPa*, from about 10 *MPa* to 1 *MPa* and that the swelling strains associated with the low saturated strength are responsible for the material cementing the rock to breakdown. The figure also indicates that little if any cementation is present after saturation and reduction of effective stress as the strength and stiffness vary in a manner consistent with an uncemented soil. As already discussed saturation and effective stress reduction lead to significant strains and these are likely to have led to the breakdown of any cementation if it were present. This result, however, does not help in determining whether the low strength of the saturated shale is simply due to the reduction in effective stress, or it is due to a combination of destructuring and effective stress reduction.

Based on the pattern of behaviour of the natural and reconstituted specimens, it can be seen that the reconstituted shale with an ultimate friction angle of 17^{o} (Section 5.4.5) gives strength comparable with the saturated natural material, which gave an ultimate friction angle of 16^{o}. The differences between the intact shale and the reconstituted

material are relatively minor, but not insignificant. This suggests that it is the structure resulting from the high compressive stresses that is responsible for the low friction angle particularly as the stress reaches more than 6 *MPa*. This has been also detected earlier from the trend of the compression lines for both natural and reconstituted material (Fig. 5.42). This is another indication that the cementation is relatively weak in this material and that the strength is controlled mostly by frictional effects. Based on the ultimate friction angle measured for the slurry form (Section 5.4.4.3), it can be suggested that this behaviour is also a consequence of the low void ratio, and associated particle alignment.

Stiffness at zero confining pressure was determined for specimens at their natural water content. Data from previous tests on saturated specimens were also analysed and the tangent modulus of elasticity, measured at 50% of the peak strength across a range of confining stresses between 0.02 to 60 *MPa* determined. However, only external displacement measurements were used to estimate the modulus of the material, and the data will have been influenced by end effects because of the difficulty of preparing specimens. The influence of saturation on natural and reconstituted material has also been investigated and compared to previously reported data on the stiffness of Ashfield shale (Ghafoori, 1995).

Table 5.3 shows values of E_{50} determined from tests on intact and reconstituted Bringelly shale. For comparison, the stiffness of Ashfield shale has also been included. For consistency, only saturated specimens of intact Bringelly shale should be compared to the Ashfield shale specimens as these were believed to be fully saturated (Ghafoori, 1995). Values from saturated Bringelly shale were found to be

Table 5.3 Values of E_{50} for Bringelly and Ashfield shale

Effective confining stress (*MPa*)	**Bringelly shale Unsaturated (*MPa*)**	**Bringelly shale saturated (*MPa*)**	**Ashfield shale saturated (*MPa*)**	**Reconstituted void ratio ~ 0.15 (*MPa*)**

0	2300	-	7700	-
0.02	-	45	7750	-
0.6	-	250	-	-
1	1500	738	7900	-
6	751	823	8100	627
60	-	2800	-	1500

about an order of magnitude lower than those reported for the Ashfield shale. The difference in these values is believed to be the result of measuring deformations of the Ashfield shale specimens internally while Bringelly shale specimens were measured externally.

The data also shows that an increase in the effective confining stress was associated by an increase in the stiffness and strength of both natural and reconstituted shale in the saturated condition. Unsaturated shale, on the other hand, has shown an opposite trend where the increase in the material stiffness and strength was a result of reducing the effective confining stress. At 6 *MPa*, where direct comparison is possible, the saturated and unsaturated materials have shown similar stiffness. However, the similar stiffness of the reconstituted and natural Bringelly shales is significantly less than Ashfield shale. At 1 *MPa* effective stress, the saturated stiffness of the Bringelly shale was reduced to about 50% compared to that of the same material in unsaturated condition. At the same effective stress, an increase of stiffness by a factor of about 10 was also observed between the reported saturated stiffness of Ashfield shale and the saturated stiffness of Bringelly shale.

These observations are consistent with the weaker cementation in the Bringelly shale compared to that of Ashfield shale and also with the presence of mixed layer clay minerals in Bringelly shale which have greater potential for swelling and physico-chemical changes than the clay minerals in Ashfield shale. Furthermore, Bringelly shale

contains less siderite than Ashfield shale in which siderite acts as an effective cementing agent. The weaker cementation in Bringelly shale is evident from many aspects of the behaviour, and in particular the similarity in the stiffness between natural and reconstituted shale at an effective stress of 6 *MPa* regardless of the state of saturation. It has been suggested that cementation is relatively weak in this material, and that significant total suctions have been measured for the natural shale. It is thus believed that pore water suctions are largely responsible for the high strength and stiffness of the natural shale at low confining stresses. As confining stress increases the suctions will reduce and it is postulated the effective stress could remain approximately constant.

The highest stiffness is indicated for the Bringelly shale at the natural moisture content at low confining stress where pore water suctions (Section 5.4.10) are most significant and where cementation is least affected by strain. In the next section, the shear modulus obtained at natural water content will be used for comparison with shear modulus of intact Bringelly and Ashfield shales obtained from direct measurements at their natural water contents.

§5.4.7.5 **Hydraulic conductivity (*k*)**

Because of the difficulty of performing direct permeability measurements, k has been determined indirectly from the parameters c_v and m_v. Laboratory studies on the reconstituted specimens (Section 5.4.1.2) have been used to estimate values for k from the isotropic consolidation response (Table 5.1), and the same indirect method has been used to estimate k values for the natural specimens (Table 5.4). Saturated natural specimens were reloaded in several stages under regulated isotropic stresses and c_v values were determined for all specimens. The data shows a consistent trend of increasing c_v corresponding to the increase in the stress level.

Table 5.4 Indirect measurements of k at different stress levels for natural shale specimens

Stress level (*kPa*)	c_v(*mm*^{2}/*sec*)	m_v (*m*^{2}/*N*)	*k* (*m/sec*)	$\Delta p'/\Delta\varepsilon_v$ (*kPa*)
600	0.069	6.2×10^{-5}	1.3×10^{-8}	1.6×10^{2}
6000	0.076	1.3×10^{-6}	2.8×10^{-9}	0.8×10^{3}
60,000	0.082	1.5×10^{-7}	3.7×10^{-10}	0.65×10^{4}

The hydraulic conductivity for the natural specimens was found to be in the range of 1.3×10^{-8} to 3.71×10^{-10} *m*/*sec* corresponding to c_v values ranging from 0.069 to 0.082 *mm*^{2}/*sec*. This range of values agrees with results obtained by Itakura (1999) who performed direct permeability tests on natural specimens of Bringelly shale. A rapid drop in the range of 4.1×10^{-7} *m*/*sec* to 8.4×10^{-10} *m*/*sec* was observed as the void ratio reduced from 0.16 to 0.11. Itakura suggested that fracture closure due to increase in the effective stress was the main cause of this rapid decrease.

The influence of the effective stress on the reducing permeability was evident when the permeability of the reconstituted shale with no fractures was compared to that of the natural shale at the same stress level. The reconstituted soil gave lower permeabilities than the natural material even at an effective stress of 60 *MPa* indicating the importance of structure, even though the stress should be high enough to close any micro-cracks. These values are lower than values reported previously for field borehole tests (e.g. Golder Associate, 1982). The reason for these lower values is believed to be the field measurement procedure which allowed 48 hours for bore saturation, as this might have enabled the shale to swell and subsequently to develop more expansion in the micro-cracks. In the laboratory, these micro-cracks were controlled by the isotropic stress acting on the material during the triaxial tests.

Based on the field permeability tests carried out by ECNSW (1982) on Ashfield shale, an average value of 1×10^{-7} *m*/sec was reported. A similar average value was also measured for Bringelly shale by Golder Associates (1982). McNally (2004) suggested that the

permeability within shale is variable due to different saturation conditions and that the low permeability of shale is primarily due to the diagenetic alteration that has filled up the small proportion of opened pore space not previously closed off by the pre-existing sedimentary load. This supports what has been suggested in the current study, that the low *k* is primarily a function of low porosity due to deep burial. McNally also suggested that the permeability of Ashfield shale is controlled by fracture intensity particularly along the contact with the underlying sandstone where shearing lines are more common.

Based on experimental data, Itakura (1999) reported that the permeability of intact Bringelly shale measured under isotropic pressure, gave values that were significantly lower than those measured in the field. This is believed to be a result of two possible processes. The first is the presence of horizontal micro-cracks which have a minor influence on the axial (vertical) measurement of flow in the laboratory, while the radial (horizontal) permeability is measured in the field tests giving rise to higher *k* values. The second process is saturation of the specimens which can lead to structural disintegration if the confining stress is too low, and hence to the overestimation of *k*.

Estimation of the saturated conductivity of natural shales is further complicated by the uncertain extent to which these micro-cracks are open in the natural shale, when not influenced by sampling, and the uncertain influence of stress level.

§5.4.7.6 **Measuring the shear modulus of the intact shale**

The shear modulus, *G*, of the intact shale was determined from triaxial compression tests and also from shear wave velocity measured by the New Sonic Viewer device, Model-5217A (Fig. 5.50). The primary motivation for performing shear modulus tests was to measure the deformation of the natural material and hence to investigate the influence of saturation and the pore water suctions on the stiffness of the shale. Shear modulus, using shear wave velocity was also determined for Ashfield shale. The current results, and previously reported data (Ghafoori, 1995) for Ashfield shale are compared to those from Bringelly shale.

Figure 5.50 The ultrasonic device used for measuring shear modulus of intact shales

The stress-strain curves obtained from drained triaxial tests were used to determine *G* values at different stress levels. For each stress level, *Poisson's ratio* was determined from the slope of ε_v-ε_a curves at the beginning of shearing where the volume change curve might be considered as the elastic response of the natural shale to the stress change (Wood, 1990). The following expression was used:

$$v' = \frac{1}{2}\left(1 - \frac{\Delta\varepsilon_v}{\Delta\varepsilon_a}\right) \qquad (5.23)$$

One special isotropic triaxial test was performed on a natural material using *HET*s to measure the axial and diametric deformation of the shale at 20 *kPa* confining stress and

hence to determine the *G* value. The *HET*s were glued onto the rubber membrane (Fig. 5.51) where direct measurements of axial and diametral strains were taken.

G_{max} was also determined using ultrasonic techniques. The device enabled a direct measurement of shear wave velocity of the rock specimens at their natural moisture

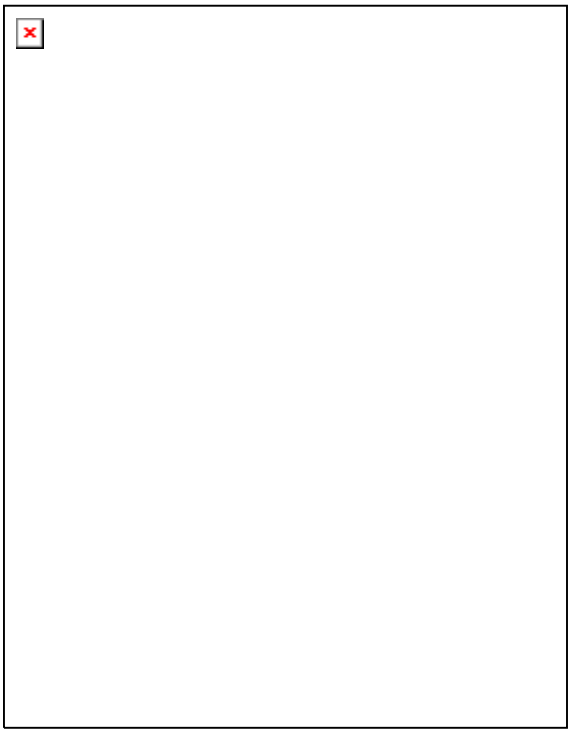

Figure 5.51 The position of the HET on the intact shale specimen

contents. In order to obtain reliable readings, a load frame (Fig. 5.52) was used to apply a low pressure to the specimens. All specimens were subjected to 35-50 *kPa* axial stress to ensure measuring a proper travelling time of secondary waves (Razouki et al., 2004).

Based on *v*' values determined from both external (stress-strain) and internal measurements (*HET*s), the shear modulus was calculated. *G* values for Bringelly shale

were determined from data obtained from the measurement of E_{50} and v' at p' ranging from 60 *MPa* to 0.02 *MPa*. Based on the data measured in Table 5.3, ε_v-ε_a relationships as demonstrated by Figure 5.53, and the expression in 5.21, the shear modulus of the natural shale was found to be in the range 1.16 *GPa*- 0.02 *GPa* respectively.

The test results from ultrasonic device were determined from the direct measurements of the time of arrival of the first shear wave for each specimen. The shear velocities

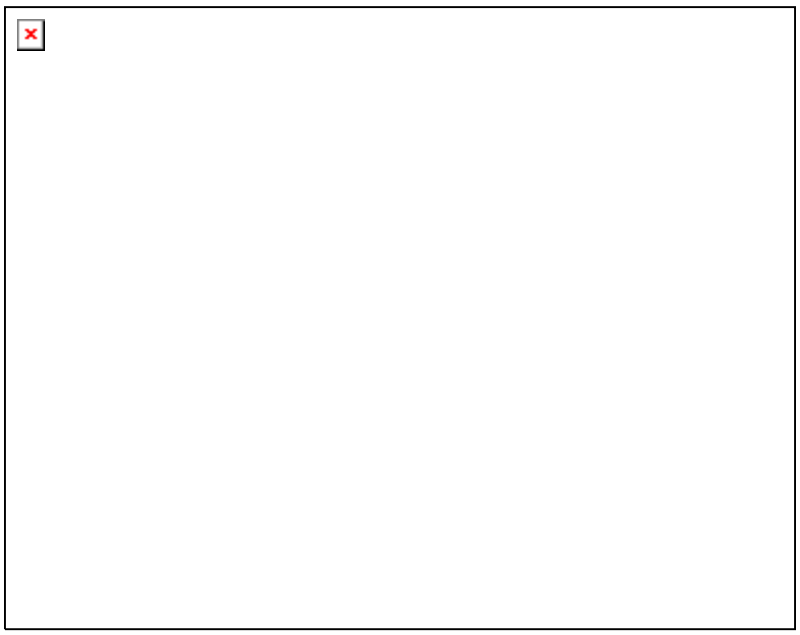

Figure 5.52 Applying force to the specimen during laboratory measurements of shear modulus using ultrasonic techniques.

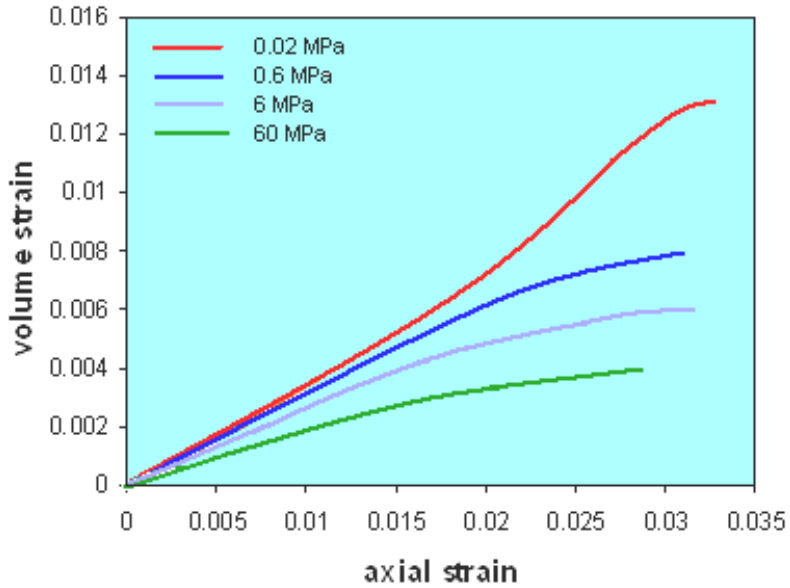

Figure 5.53 Influence of effective confining stresses on the volumetric and axial strains for saturated natural specimens

and hence *G* values were then calculated from Eq. 5.19. Data on measured parameters for Bringelly and Ashfield shales including time, velocity, height, and *G* modulus is shown in Table 5.5. These results will be discussed in Section 5.4.9

Table 5.5 Data measured by ultrasonic device showing comparison between Bringelly and Ashfield shales

Bringelly				**Ashfield**			
Time *(μsec)*	**Specimen height (*m*)**	**Velocity (*m/s*)**	**Modulus (*GPa*)**	**Time *(μ sec)***	**Specimen height (*m*)**	**Velocity (*m/s*)**	**modulus (*GPa*)**
62.4	0.091	1458	3.5	59.2	0.095	1605	4.1
63.2	0.072	1139	2.8	19	0.032	1684	4.3
56.8	0.074	1303	3.2	25.6	0.047	1835	4.7

§5.4.8 **Discussion**

The testing programme described in this section was carried out to investigate the strength and stiffness of the natural shale. It has been suggested that the shale is weakly cemented, and yet *UCS* value of up to 50 *MPa* have been measured. An important aim of these tests was thus to help understand the mechanisms that lead to these apparently

contradictory observations. In addition the reconstituted specimens have indicated lower friction angle of 17^o applies at low void ratios compared to 28.5^o at higher void ratios, and the effective friction angle of the saturated natural shale was unexpectedly much less than that of the reconstituted shale. A series of tests on saturated and unsaturated specimens were also carried out to investigate the influence of saturation on the behaviour of the natural shale.

Based on the pattern of behaviour of the natural and reconstituted specimens, it can be seen that the reconstituted shale with an ultimate friction angle of 17^o (Section 5.4.5) gives strength comparable with the saturated natural specimens, which gave an ultimate friction angle of 16^o. The differences between the intact shale and the reconstituted material are relatively minor, but not insignificant. This suggests that it is the structure, resulting from the high compressive stresses, that is responsible for the low friction angle. The compaction stress of the natural shale has also been estimated earlier from the trend of the compression lines for both natural and reconstituted material (Fig. 5.42) and found to be explainable from the sediment burial. This is another indication that the cementation is relatively weak in this material and that the strength is controlled mostly by frictional effects.

The natural shale has a very low porosity, similar to that produced by reconstituted shale specimens subjected to high stresses. The low friction angle measured for natural shale was consistent with the value measured for the reconstituted shale, suggesting the role of particle alignment in applying the same mechanism on both natural and reconstituted specimens (further discussion later in this section). In addition, natural material has significant micro-cracking in the plane of the laminations. Consideration of this factor would also suggest that the effective friction angle controlling the strength of the shale could be further reduced. For instance, it is possible that tests on natural shale cores oriented at other angles to the vertical may show even lower frictional strengths when failure surfaces are aligned with the micro-cracks.

The effect of saturation on the intact Bringelly shale was pronounced as it led to significant reductions in the strength and stiffness for confining stresses less than about 6 *MPa*. Stiffness data from reconstituted and natural Bringelly shale were obtained from external and direct measurements. External measurements were based on data measured by external devices such as *GDS* and *LVDT* and stress-strain responses during the isotropic triaxial tests. In these tests, stiffness was based on tangent values measured at a deviator stress of approximately 50% of the peak strength. Internal devices such as Bender elements and *HET*s were also used to measure shear modulus. An ultrasonic device was also used to measure the shear modulus at very small strains of the intact Bringelly and Ashfield shales.

Depending on the applied confining stress, the stiffness of the saturated natural material varied from 2.8 *GPa* to 45 *MPa* as the confining stresses were reduced from 60 *MPa* to 20 *kPa* (Fig 5.54).

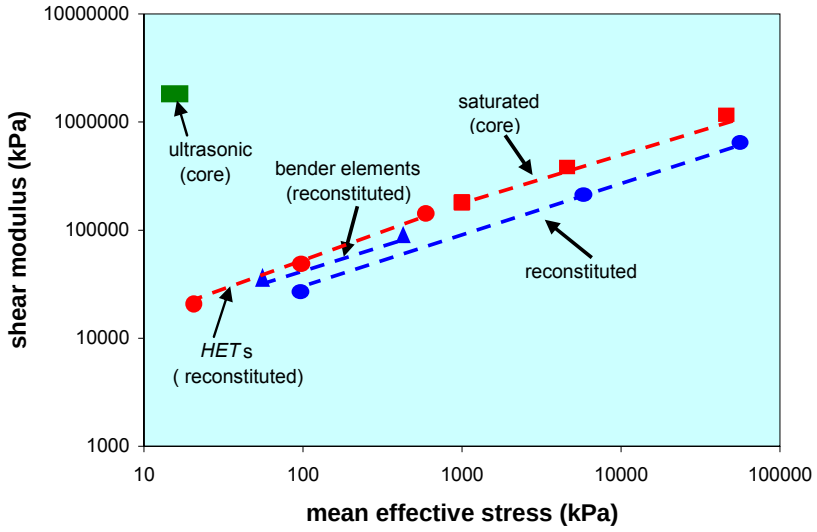

Figure 5.54 Influence of stress on the stiffness of Bringelly shale

This behaviour was inverted when stiffness of the material was measured at its natural water content, with the stiffness reducing with increasing stress. This change in behaviour

shows the influence of confining stress in improving the degree of saturation of the natural shale by 30-40% and hence reducing its stiffness. The reconstituted material showed a significant increase in the stiffness when the confining stress was increased from 6 *MPa* to 60 *Mpa*, similar to that demonstrated by the saturated natural material.

Evidence for weak cementation in the natural Bringelly shale has been demonstrated by the similar stiffness of the natural and reconstituted shale at the same confining stresses and at similar porosities. It has been observed that Ashfield shale, which is more cemented, has similar values of stiffness to the Bringelly shale at its natural moisture content when tested by the ultrasonic device. It is believed that high suctions contribute to the stiffness of Bringelly shale, but suctions have been shown to be lower for the Ashfield shale, where the cementation component of stiffness is more important.

In addition to the use of the external measurements to measure shear modulus, G, special tests involving the use of Bender elements, *HET*s, and shear wave velocity were also performed to measure the same parameter. The outcomes of these tests are plotted on a log-log graph in Figure 5.54. The figure shows the stiffness of the natural and reconstituted material obtained from different techniques. No direct measurements of G by the Bender elements could be obtained for the natural material due to the difficulties in creating a slot for the benders. However, *HET*s were used to measure G_{max} of the natural shale at a confining stress of 20 *kPa*. The shear modulus at this low level was found to be about 1800 *kPa*. This low value reflects the influence of saturation in reducing the stiffness of the material and also the influence of the swelling due to the stress release the material has experienced before shearing. This is another indication of the weak cementation bonds of the natural shale.

§5.4.8.1 **Evaluation of the experimental techniques**

The influence of void ratio on the stiffness of the reconstituted material can also be investigated using the same figure. At low void ratio of ~0.15, the material demonstrated much higher stiffness than that shown by the same material at a void ratio of 0.5.

However, this is primarily due to the greater stress level at low void ratio. On unloading to OCR = 10 the stiffness of the reconstituted soil was similar to that on initial loading, suggesting that void ratio and particle arrangement have relatively minor effects on stiffness. The influence of external measurements can also be observed in Figure 5.54 from the difference in the stiffness of the reconstituted material at mean effective stresses of up to 400 *kPa* when compared with the bender elements. The latter show a higher stiffness than the one measured with the external devices. Figure 5.54 also shows that the *G* values based on the pre-determined *v'* from the external (ε_v- ε_a) and internal measurements (*HET*s) are less than those directly measured by the ultrasonic device by at least an order of magnitude. The difference in *G* values compared to those determined from the shear wave velocity can be partly explained by the limitations of external stiffness measurement. However, for reconstituted specimens the bender element results indicate that the external measurements are only slightly underestimating G_{max}. Another possibility is that the ultrasonic tester is giving erroneous results, but this appears unlikely as for Ashfield shale, the results from the ultrasonic device were consistent with those reported by Ghafoori (1995), obtained from gauges attached directly to the specimens. It has previously been suggested that both the high suction and weak cementation contribute to the strength and stiffness of the Bringelly shale. The high shear wave velocity at the natural moisture content appears to indicate that some cementation must be present as extremely high suction would be required to explain the stiffness purely from differences in effective stress.

Stiffness is sensitive to the presence of cementation. This property can play an important role in assessing the nature of the cementing agent of the material (Atkinson et al. 1993). This was evident from the trend of the stress, strain curves of saturated and unsaturated specimens at different effective confining stress (Figs. 5.43, 5.48a,b) The trend shows a marked difference in the linearity of the stress-strain curves of the specimens at different saturation conditions. The saturated tests give a linear trend while the unsaturated tests show very non-linear behaviour. It is not known if the linearity is a function of stiffness or the influence of saturation on the cementation of the material. However, the trend

shows that the initial stiffness is not greatly affected by either the effective stress or the degree of saturation. This suggests some cementation is present in the shale.

A related study, concerned with the behaviour of highly plastic intensely fissured clay shales from Italy, has been presented by Picarelli et al (1998, 2003). They show that the normalised state boundary surface of the intact shale lies below the surface of the reconstituted material. Picarelli et al. related the behaviour to the effects of fissuring in the natural soil and suggested that the mechanism of deformation could be described by the classical model used for fractured rocks, where deformation and strength are controlled by movements along joints and fissures. They also reported the insignificance of *OCR* in influencing the strength of the material. The same pattern of behaviour reported by Picarelli et al. can be seen in Figures 5.18, 5.27, 5.28, 5.32, and 5.33. The observation that the highly compressed reconstituted shale also has a low frictional resistance suggests that the fabric associated with the low porosity, created by the high stress, is also contributing to the reduced frictional strength and different deformation mechanisms. At low porosity there must be locally a high degree of alignment of the plate-like clay particles. It is possible that failure surfaces could develop that pass through regions where the particles are highly aligned.

The mechanism suggested is illustrated in Figure 5.55, and is identical to that proposed by Picarelli et al (1998) for their fissured shale. The effective friction angle

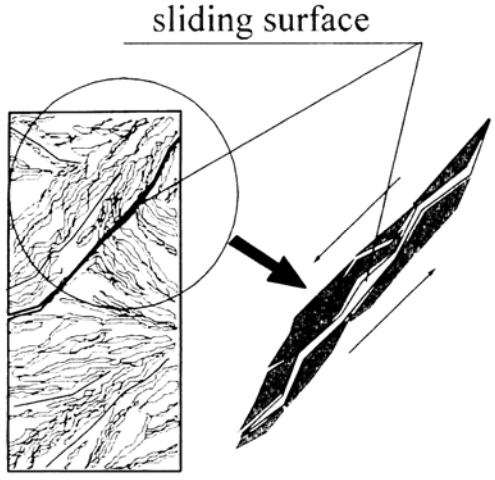

Figure 5.55 Mechanism of shear deformation and rupture
(after Picarelli et al, 1998)

is controlled by the interparticle friction angle between the particles, ϕ_u, and the effective dilation angle, which will depend on the roughness of the failure surfaces. It is postulated here that this mechanism is controlling the behaviour of the low porosity reconstituted material even though fissures are not present. The natural Bringelly shale has a very low porosity, similar to that produced by the high stresses in this study.

A comparison of the drained stress-strain responses of the reconstituted material and the intact shale at an effective stress of 6 *MPa* has revealed that the stiffness and strength of the natural shale are only slightly greater than the reconstituted material which is contradictory to the rock mechanics procedure that would classify the shale as a strong rock. In addition, at confining stresses of 6 *MPa* and above there is no difference in the ultimate friction angles of the reconstituted and natural material. At lower confining stress, the strength of the intact shale is a function of the saturation condition of the material.

Scanning electron micrographs have shown that the intact shale has highly aligned clay particles and this suggests a mechanism for the low strength and stiffness based on sliding between agglomerations of clay particles. *SEM* pictures were taken before and after shearing in an attempt to identify the fabric and mechanisms responsible for the low frictional strength in the compacted shale. Examples of images taken after shearing are shown in Figures 5.56 and 5.57. Figure 5.56 shows an overview of particle alignment for a specimen at 60 *MPa* as it is demonstrated by the parallel bands. When magnified, particle alignment along the failure plane is produced as indicated by the red arrows (Fig. 5.57). The micrograph shows diagonally aligned parallel bands resulted from a strong alignment of the clay platelets due to the high

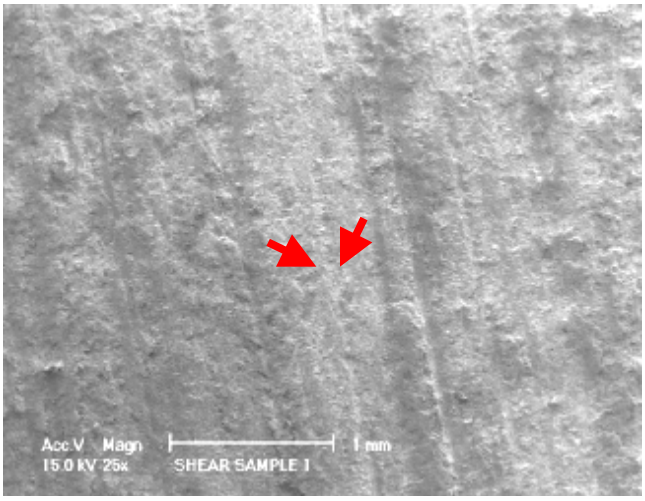

Figure 5.56 Section at the shear plane of rock specimen at high stress, viewed normal to the shear plane (Magnified at 25x)

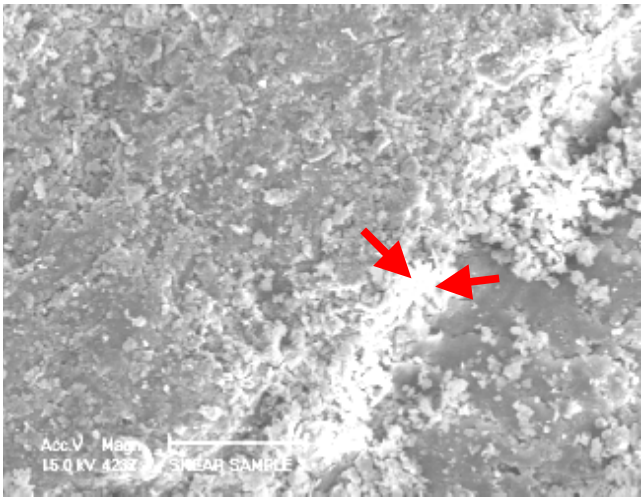

Figure 5.57 Magnified image of parallel bands of clay platelets at high stress, viewed normal to the shear plane (Magnified at 1000x)

stress level. This pattern was not clearly defined (Fig. 5.58) as no parallel bands have been detected when the specimen was subjected to a low stress during shearing.

Micrographs were also taken of sections in the specimens that were free of shear bands (e.g. Fig. 5.59). The figure shows no particular pattern that might suggest particle movements in any one direction. This may affirm the heterogeneity of the material when subjected to high stresses. However, it is worth mentioning though that at a confining stress of 6 *MPa*, the stiffness of the natural and reconstituted shales are similar.

This was also evident from the poor alignment of the plate-like clay particles at a stress level of 6 *MPa* (Fig. 5.60). This poorly identified pattern of alignment is similar to that for specimens subjected to even lower stresses (Fig. 5.61). In order to obtain a wider exposure to figure, the specimen was tilted at a different angle prior to scanning. It can be stated that no identifiable pattern of alignment was observed at stresses ≤ 6 *MPa* prior to the isotropic compression of the natural shale specimens.

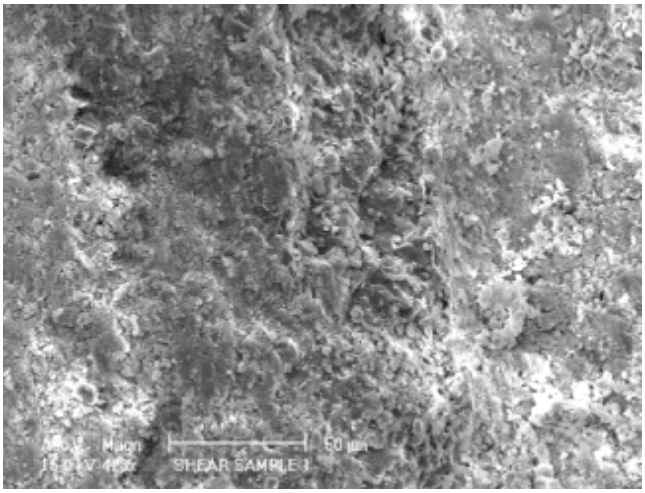

Figure 5.58 Magnified image of undefined pattern of clay platelets at low stress, viewed normal to the shear plane (Magnified at 1000x)

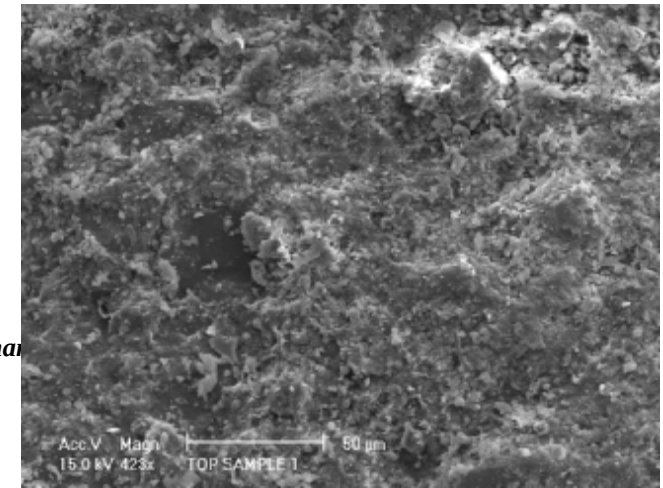

Figure 5.59 Rupture free section at the top portion of a specimen subjected to a high stress of 60 *MPa*, viewed normal to lamination (Magnified at 1000x)

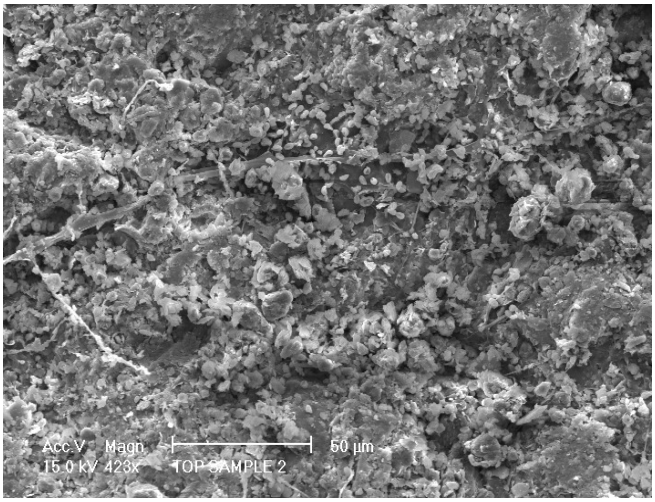

Figure 5.60 photomicrograph of a specimen subjected to 6 MPa (Magnified at 1000x)

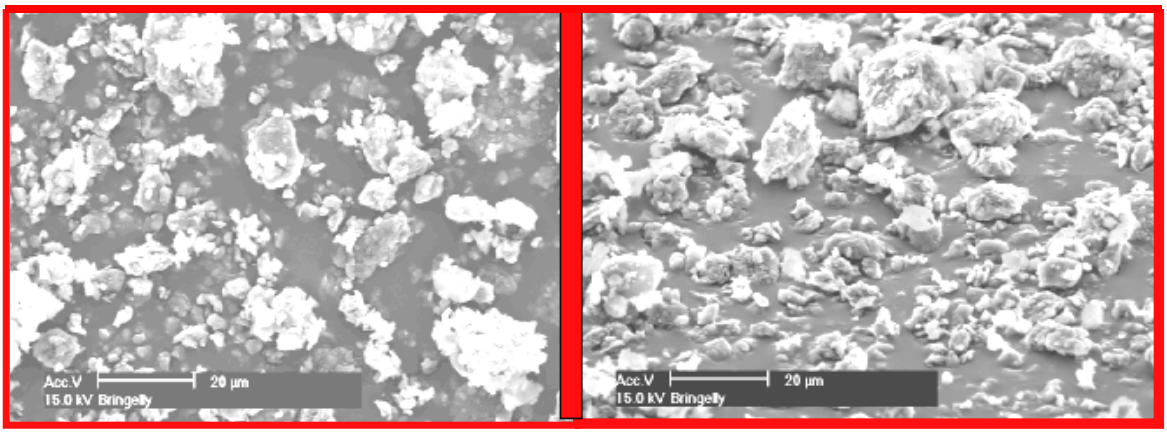

specimen oriented at zero degree specimen oriented at 45 degree

Figure 5.61 Stacking of platelets of natural shale at unconsolidated state

§5.5 RESIDUAL SHEAR RESPONSES

§5.5.1 Introduction

In this study, it has been observed that void ratio has a crucial effect on the friction angle. For $p'_c < 6\ MPa$ and $e > 0.23$, an ultimate ϕ' of 28.5° was measured. For $p'_{c\ max} = 60\ MPa$ and $e \leq 0.15$, the measured ϕ'_{ult} was only 17°. A similar low ϕ'_{ult} of 16° was measured for the natural shale. It is believed that the low strength at low void ratio is related to particle alignment. It might therefore be expected that the residual strength of this material would be given by $\phi_r \approx 17°$ as when a residual strength lower than ultimate is measured this is related to particle alignment (e.g. Lupini et al., 1981). For soil with clay content > 40% significant differences between peak and ultimate ϕ' can be observed (Skempton, 1985). Two series of tests were performed using direct shear box and ring shear apparatus to determine the residual strength at low confining stresses. A brief summary of the equipment, specimen preparation, and test results are given in the following sections.

§5.5.2 **Ring shear test**

The small ring shear apparatus used in this study uses an annular ring shaped specimen in which the lower half is rotated whilst the upper half is held stationary (Bromhead, 1979, 1986). The soil specimen used in this study was prepared from the reconstituted shale whose physical properties have been given in Section 4.2. An annular soil specimen 5 *mm* thick with inner and outer diameters of 70 and 100 *mm* respectively was confined radially between concentric rings (Fig. 5.62). It was then compressed vertically between porous bronze loading platens by means of a lever load system and dead weights (Fig. 5.63). The specimen with the particles passing through 425 μm size sieve was prepared in situ in the apparatus. It was mixed with tap water to a slurry at the plastic limit. To ensure saturation of the specimen, the soil was submerged in tap water at all times.

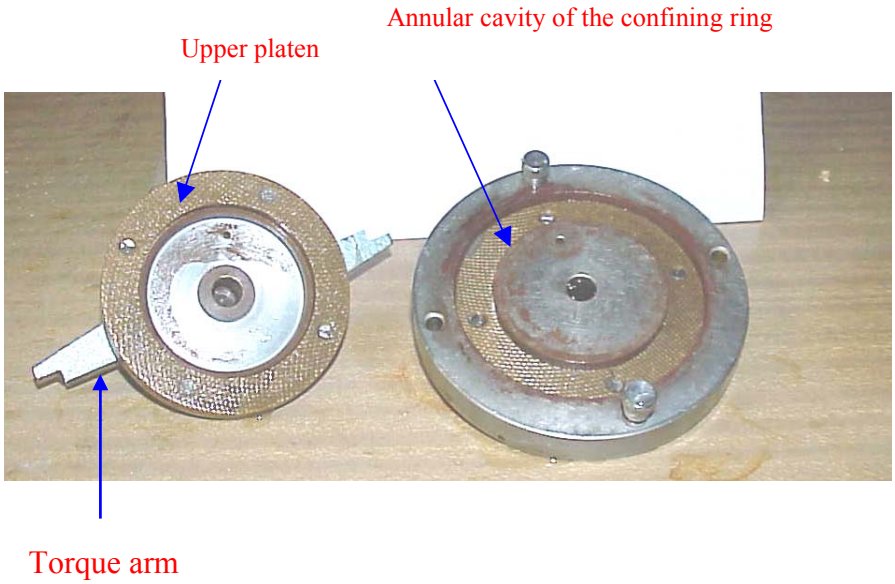

Figure 5.62 Sample compartment of a simple ring shear apparatus

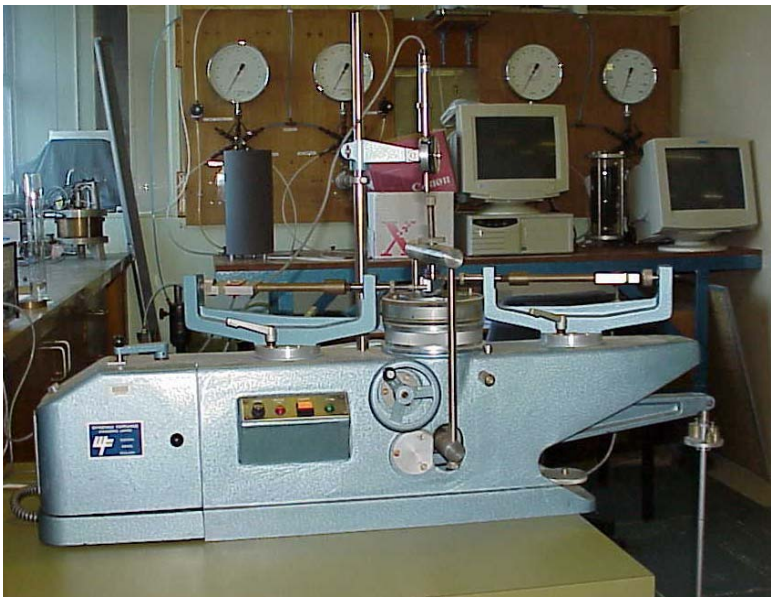

Figure 5.63 General arrangement of ring shear apparatus

The specimen was then subjected to staged consolidation prior to the commencement of shearing. The excess pore pressure generated during the formation of the shear plane was allowed to dissipate slowly for a period of two hours.

To prevent swelling of the material, a vertical force was applied for 24 hours to produce a vertical stress of 10 *kPa*. After this, a shear plane was formed by rotating the specimen two revolutions using a hand wheel for a period of 1 minute.

All tests were performed with a shear displacement rate of 0.048 *mm/min* and at angular velocity of 0.037^{o} / *min* as recommended by Bromhead (1979). In order to prevent the prepared specimen from being squeezed out between the confining rings and the upper platen, it was necessary to consolidate the specimen in several stages.

In order to minimize the friction between the upper and lower rings and the outflow of the specimen from the shear surface, the gap between the upper and lower rings was fixed at 0.2 *mm*. During the test, time (*T*), vertical dial gauge (*VDGR*), and torque ring dial gauges (*LLC*, *RLC*) were monitored and recorded in units of minutes, millimetres, and newtons respectively. All readings were recorded at regular intervals of the angular rotation (θ). A minimum of 20 sets of readings were taken in each shear stage. The test was stopped when the residual state had been reached. The shear strength was calculated according to the following formula, derived by Bromhead (1979):

$$\tau = 0.436\ (\ LLC+RLC) \qquad (5.24)$$

Following the end of the shearing stage, the torque was then reduced to zero. The specimen was then consolidated to the next normal effective stress. Three different normal stresses were employed for each specimen in this study, 50, 100, and 200 *kPa*.

§5.5.3 **Direct shear test**

A series of direct shear tests on specimens, each under a different normal load to determine the residual friction angle of the material were also carried out. A schematic illustration of the principle of the test is shown in Figures 5.64a,b.

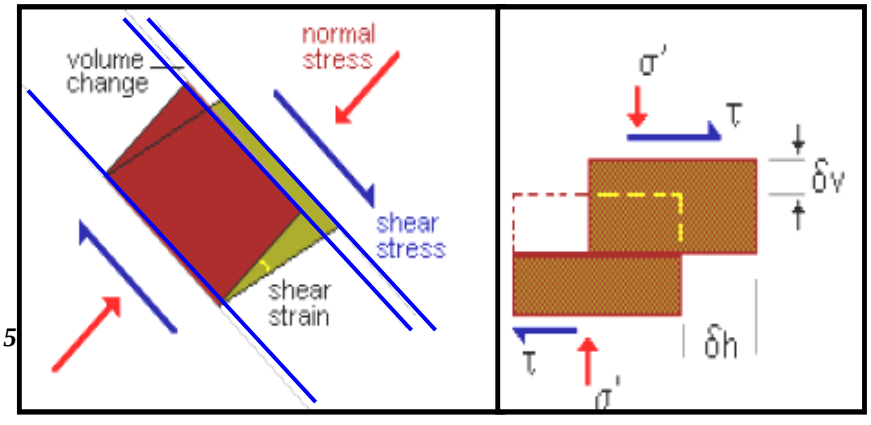

a b

Figure 5.64 Diagrammatic illustration of the principle in shear box in simple shear (a) and direct shear (b)

The tests were performed in an automated square shear box apparatus (Figure 5.65). The square shear box with an area of 3600 mm^2 is divided by a horizontal plane into two halves of equal thickness which fit together with alignment screws. Gap screws are also fitted to control the space between the top and the bottom halves of the box.

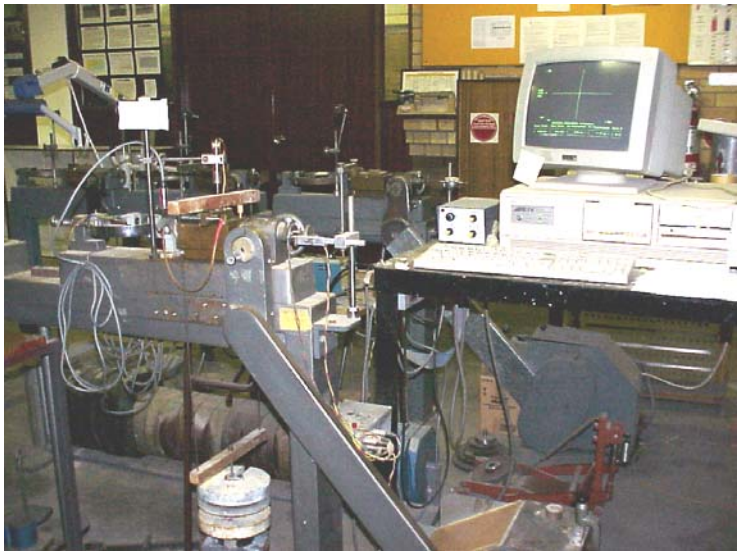

Figure 5.65 Overview of the automated shear box apparatus

The specimens used for these tests were prepared from the reconstituted shale to form a slurry at the liquid limit. Slurry was placed in the shear box with well greased side walls and compressed one-dimensionally by staged increase of the normal load. The tests were carried at 50, 100, and 200 *kPa* normal stress levels. Based on the consolidation characteristics of the material, a slow strain rate of 0.03 *mm*/*min* was used. For each test, the specimen was submerged at all times to keep it saturated and to reduce the possibility

of generating excess pore pressure. During the tests, all variable parameters and their devices were monitored and data readings were automatically recorded. The method of preparation and procedure of this test series were carried out in accordance to *ASTM Standard D*30-90 (1996).

§5.5.4 **Experimental results**

For each apparatus representative graphs showing shear displacement (δh) and normal displacement (δv) against shear stress (τ) were plotted. For ring shear tests, the horizontal displacement was calculated from the measured angular displacement in accordance with the British Standard for determination of residual strength using the small ring apparatus (Bromhead, 1979; BS 1377: 1990).

A typical relationship between shear stress and horizontal displacement in a shear box apparatus is illustrated in Figure 5.66.

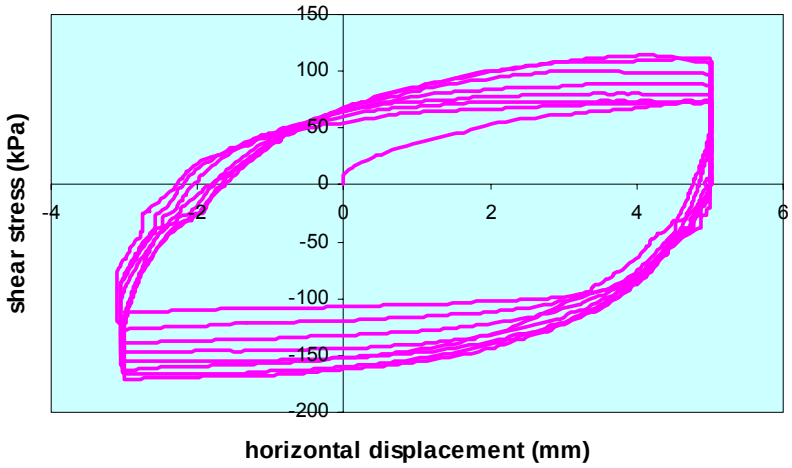

Figure 5.66 Shear box response at 200 kPa normal stress

Similar responses were obtained in the other tests at 50 and 100 *kPa*. The figure shows that cycling with displacement amplitude of 4 *mm* was used. It also shows the resistance

in each cycle gradually increased until a steady state appeared to be reached after 8 cycles. No evidence of reduction towards a residual state was obtained. Tests were stopped after 8 cycles because of concerns about loss of material and tilting of the top half of the apparatus. In the ring shear test, shear stresses for each applied normal stress were calculated and plotted against the linear horizontal displacement (Figure 5.67). The figure shows that the resistance is very much influenced by the applied normal stress.

In order to determine the residual friction angle from the two experiments, the strength envelopes of the test results from the shear box and the ring shear were plotted (Figure 5.68). In order to define the residual friction angle, the ultimate shear

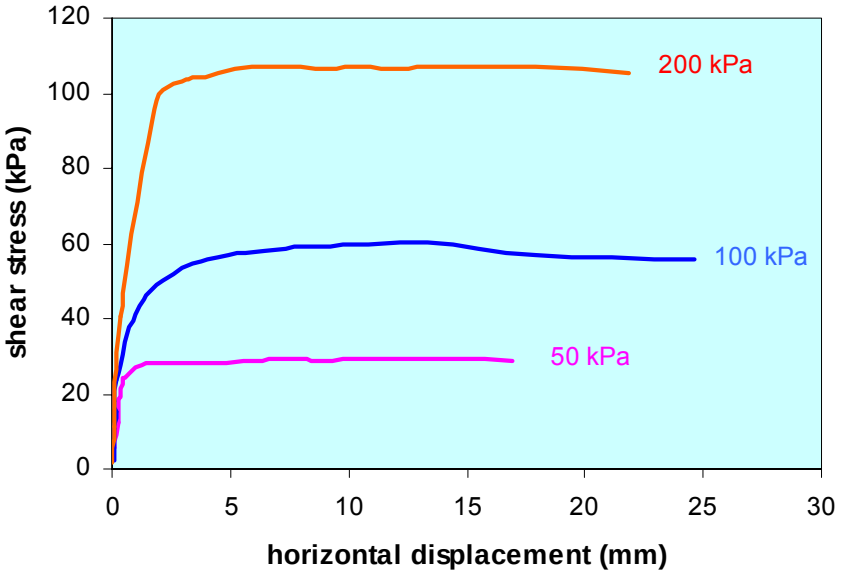

Figure 5.67 Relationship between shear stress and linear shear displacement in a ring shear test at different stress levels

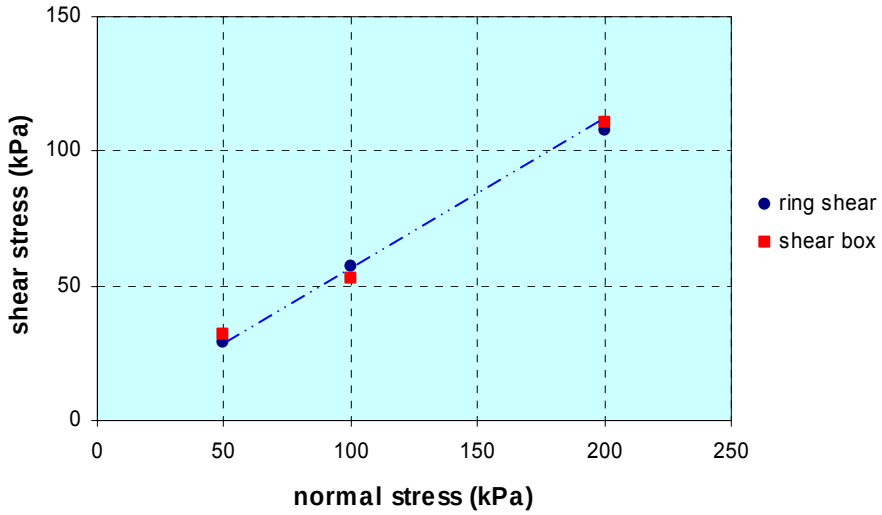

Figure 5.68 Strength envelopes of reconstituted soil

stresses for both ring shear and shear box were plotted against the applied normal stresses for each test. Based on the Mohr-Coulomb criterion, the residual shear strength was defined by the expression:

$$\tau = c_r + \sigma \tan \phi_r \qquad (5.25)$$

in which

c_r is the cohesion at residual shear strength, and

ϕ_r is the friction angle at residual shear strength

The residual friction angle obtained from the test results of both ring shear and shear box was 28.2^0, while c_r was approximately zero. This value agreed with the critical

state friction angle obtained from the stress paths of the low pressure test series (≤ 6000 *kPa*) on reconstituted specimens.

§5.5.5 **Discussion**

Although different methods of testing and preparation were used for shear box and ring shear tests, both gave identical residual strength. This is an indication that loss of material from the shear plane in the apparatus was probably not significant.

For this material, a peak strength was generally obtained at a small displacement, and a reduction of strength to a critical state value was associated with further displacement and ultimately without further change in volume. Based on the measured clay content of the material (51%) particle reorientation may occur, and this could result in further reduction in shear strength until the material approaches a residual strength. However, the test results show, $\phi_r = \phi'_{ult}$ for the low pressure series, indicating that despite the high clay fraction content of the material, the residual friction angle has not been affected by the reorientation of clay particles.

Despite the different geometry and different normal stresses acting on the material during shearing, the reconstituted Bringelly shale demonstrated similar behaviour when tested in the triaxial cell, the shear box, and the ring shear. This was evident from the similar values of critical state friction angle and the residual friction angle obtained from the tests performed on the reconstituted material. The agreement of these results strongly implicates the porosity for the reduction of the effective friction angle at high stresses or low porosity. At low porosity, there must be regions with a high degree of alignment between the plate-like clay particles. Through these regions, failure surfaces could develop where the particles are highly aligned.

Particle size analysis (Section 4.2.3) has indicated that 50% of the Bringelly shale content has platy shape particles, while the remainder is particles with a more rounded shape. This grain size distribution in the shale material may explain the mechanism of the turbulent mode the material experienced during shearing. It is believed that at high porosity, the platy particles are poorly aligned as the rounded particles of silt size managed to prevent alignment of clay particles on the shear surface and that the effects of

clay particles are overridden by the predominance of silt around the shear surface causing the rolling shear. The impediment to the platy shape particles aligning near the shear plane is believed to have resulted in obtaining shear strength similar to the peak strength. At low porosity, the mechanism of failure is different where the high degree of alignment of the clay platelets near the shear surface (Section 5.4.10) is sufficient to produce a sliding shear mechanism.

Various attempts have been made to correlate the residual strength friction angle ϕ'_r of soils to their index parameters. Lupini et al. (1981) pointed out that correlations between residual strength and soil index properties cannot be general. Based on their investigation, they also suggested that there is discontinuous change in the relationship of ϕ' to *PI* at a *PI* of about 30. In an effort to re-establish the Lupini et al. observations, Wesley (2003) used the Atterberg-limit chart to correlate between its parameters and the residual friction angle. He used the distance ΔPI above or below the *A-line* as indicative of the ϕ'_r measurement. This distance is given by:

$$\Delta PI = PI - 0.73(LL - 20) \qquad (5.26)$$

The trend of the soil behaviour indicates that soils lying well above the *A-line* will have very low ϕ'_r whereas those positioning well below the *A-line* can be expected to have high ϕ'_r. Based on the plotted data from Bringelly shale on the consistency chart (Fig. 4.7) and the calculated distance from the *A-line*, the residual friction angle on Wesley chart was about 28^o. This value agrees well with the ϕ'_r value obtained from the ring shear results. The compliance of the data with Wesley's chart is interesting as Wesley suggested that his graph is only applicable for soils with $LL > 50$. It is worth mentioning here that Bringelly shale has low plasticity and *LL* significantly less than 50 (Section 4.2.4).

As the current studied material contains > 50% clay fractions, it is believed that the reorientation of clay particles at stress < 1000 *kPa* was not achievable and therefore no reduction in the shear strength was attained despite the large displacement the specimens have experienced (Section 5.4.5). Specimens that were subjected to high stress level have exhibited a reduction in their shear strength due to the reorientation of the clay platelets. However, these observations may suggest the need for more soil varieties to be tested in order to establish a strong correlation between index properties and residual strength of the soil materials.

§5.6 **SUMMARY**

Slurry, dry press, and core forms were used to investigate the behaviour of the shale under isotropic confining stresses. Different techniques were used to prepare the specimens prior to their testing in the triaxial equipment. The consolidated drained and undrained tests performed on the reconstituted shale involved stages of isotropic compression/swelling to values ranging between 20 *kPa* to 60 *MPa*. Drained tests were also performed on natural shale. The slurry specimens when subjected to a maximum effective confining stress of 1000 *kPa* showed the expected patterns of behaviour for a clayey soil, with a critical state friction angle of 28.5°. Critical state

friction angles and internal friction angles calculated from the effective stress paths of saturated natural and reconstituted specimens were plotted in ln (p') - ϕ space (Fig. 5.69).

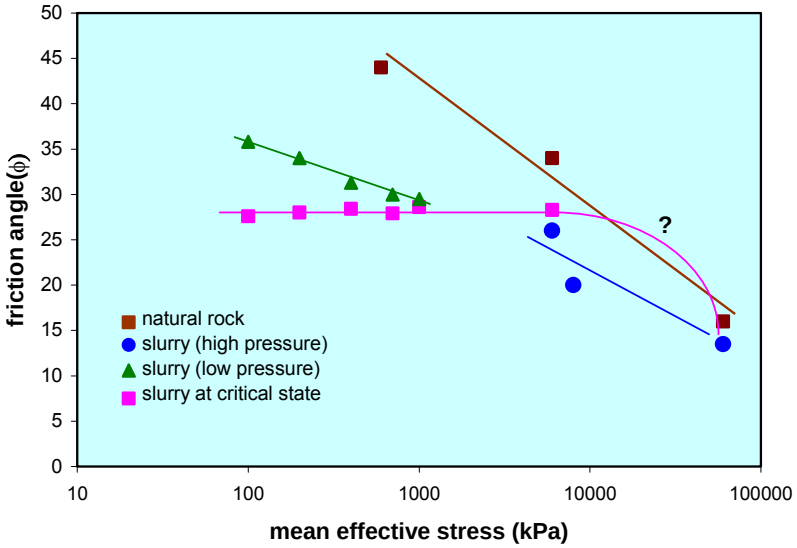

Figure 5.69 Influence of stresses on reconstituted and natural shale at saturated condition

The figure shows relationships between the mean effective stresses and friction angles at different conditions for reconstituted and natural specimens. Lines of best fit were drawn to show the trend of data points for each test series. The critical state friction angle of the reconstituted specimens is consistent up to a confining stress of 6*MPa*. However, at higher confining stresses, the frictional strength of the saturated reconstituted shale decreases. The rate at which the friction angle decreases (indicated by ?) is uncertain as no data were obtained between 6*MPa* and 60*MPa*. It may be noted that departure from the linear INCL occurred at 10*MPa*, which is similar to the pressure at which the friction angle starts to reduce. It can be seen that the reconstituted shale gives strength comparable with the natural material, a frictional strength of 17^{o}, when it is compressed to the same void ratio. The graph also shows the behaviour of the overconsolidated reconstituted shale at different preconsolidation stresses as indicated by the green and blue data points at failure. With a maximum mean effective stress of 1*MPa* (green line), the material demonstrated an increase in the effective friction angle at lower effective stresses. A similar behaviour was demonstrated by the reconstituted material at maximum preconsolidation stress of 60 *MPa* (blue line). Both trends comply with the overconsolidated behaviour in soil mechanics (i.e. an increasing peak strength with overconsolidation ratio).

For the partially saturated shale, the material was subjected to a maximum confining stress of 60*MPa*. The trend of the line shows a significant reduction in the friction angle with confining pressure, but because the sample is partially saturated, the true effective frictional strength can not be estimated as the suction prior to and at failure is unknown. Although the trend of the line for the partially saturated shale agrees with that of the reconstituted shale, the frictional strength of natural shale is not directly comparable to that of the reconstituted material.

It is worth mentioning here that an increase in the confining stress would tend to reduce the suction in the material. This may lead to a subsequent reduction in apparent cohesion and friction of the material. When the sample was saturated, a reduction in strength was evident. Further investigation in which the suction is measured would improve the understanding of the mechanism involved.

The presented data show also difference in the strength parameters between the reconstituted and natural specimens at the same effective stress. The variation in the strength is due to the low porosity of the natural shale that led to a high degree of alignment of the clay particles and yet to the increase in frictional strength particularly for the natural specimens. The outcomes of these tests agree with results reported by other authors (section 2.4.8) and confirm that friction angles in shale rock is influenced by the softening condition of the material and also by the roughness of the failure surfaces.

The slurry specimens when subjected to effective confining stresses of 60*MPa* showed behaviour that was not consistent with the assumptions of critical state soil mechanics, and indicated an ultimate friction angle of 17^{o}. Tests performed in shear box and ring shear apparatus have indicated that the incomplete clay particle reorientation in low pressure test series has resulted in critical state / ultimate state friction angle being equal to the residual friction angle. For the high pressure test series, reorientation of clay particles is believed to have occurred, and the reduction in shear strength is significant.
Similar patterns of behaviour were repeated when natural shale was reloaded to the same range of effective confining stresses. The natural shale has a very low porosity, similar to that produced by the dry press specimens and specimens subject to high stresses. Triaxial tests were performed on shale at the in-situ water content, on the natural shale after saturation, and on material that was reconstituted. It has been found that the reconstituted material, after compression to high stress levels so that its void ratio is comparable with the natural shale, gives strengths and stiffness comparable to the natural shale.

Permeabilities were measured for reconstituted and natural shale specimens at different stress levels. At a maximum effective consolidation stress of 60*MPa*, the hydraulic conductivity of natural shale was less than that of reconstituted specimens. This was indicative from the difference in the c_v values of 0.082 mm^2 / *sec* and 0.065 mm^2 / *sec* respectively. This result agrees with the difference in the void ratio of the intact and reconstituted shale at this high stress level which are 0.1 and 0.15 respectively. The results also show that very dramatic increases in permeability can occur if Bringelly shale is free to swell.

In the current study, it has been suggested that the path developed by the failure surfaces during the triaxial tests is related to the high alignment of the platy clay particles. This supports the role of mineralogy of the clay in influencing the residual strength of the material, particularly when the clay fraction exceeds 50% (Lupini et al., 1981). At low porosity, the platy structured minerals such as illite, montmorillonite, and chlorite are strongly aligned along the shear plane. Their thin plates and weak inter-particle bonds accommodate more stacking and cause a reduction in the peak strength.

The degree of saturation affects the strength and slightly the stiffness of the material. Degree of saturation and stiffness are related properties that can influence the frictional strength and cohesion of shale. The relationship between the two properties can be used to suggest the cementing condition of the material. An important factor controlling the strength and stiffness of Bringelly shale appears to be pore water suction. Despite reasonably high degrees of saturation, the shale has a very high total suction. When the shale is saturated and subjected to reduction in effective stress, the strains associated with saturation and removal of suction lead to reduction in strength and stiffness. This can be explained if the material cementing the rock breaks down. However, the relation between pore pressure suction, and stiffness and strength needs further study before the extent of the cementation can be reliably determined.